UNIVERSITÄT BERN

UNIVERSITÄT BERN

AEC
ALBERT EINSTEIN CENTER
FOR FUNDAMENTAL PHYSICS

LOWER BOUND ON THE PROTON RADIUS & PROTON-POLARIZABILITY EFFECTS IN MUONIC HYDROGEN

Franziska Hagelstein (AEC Bern)

in collaboration with

V. Lensky and V. Pascalutsa (JGU Mainz)

PROTON RADIUS PUZZLE

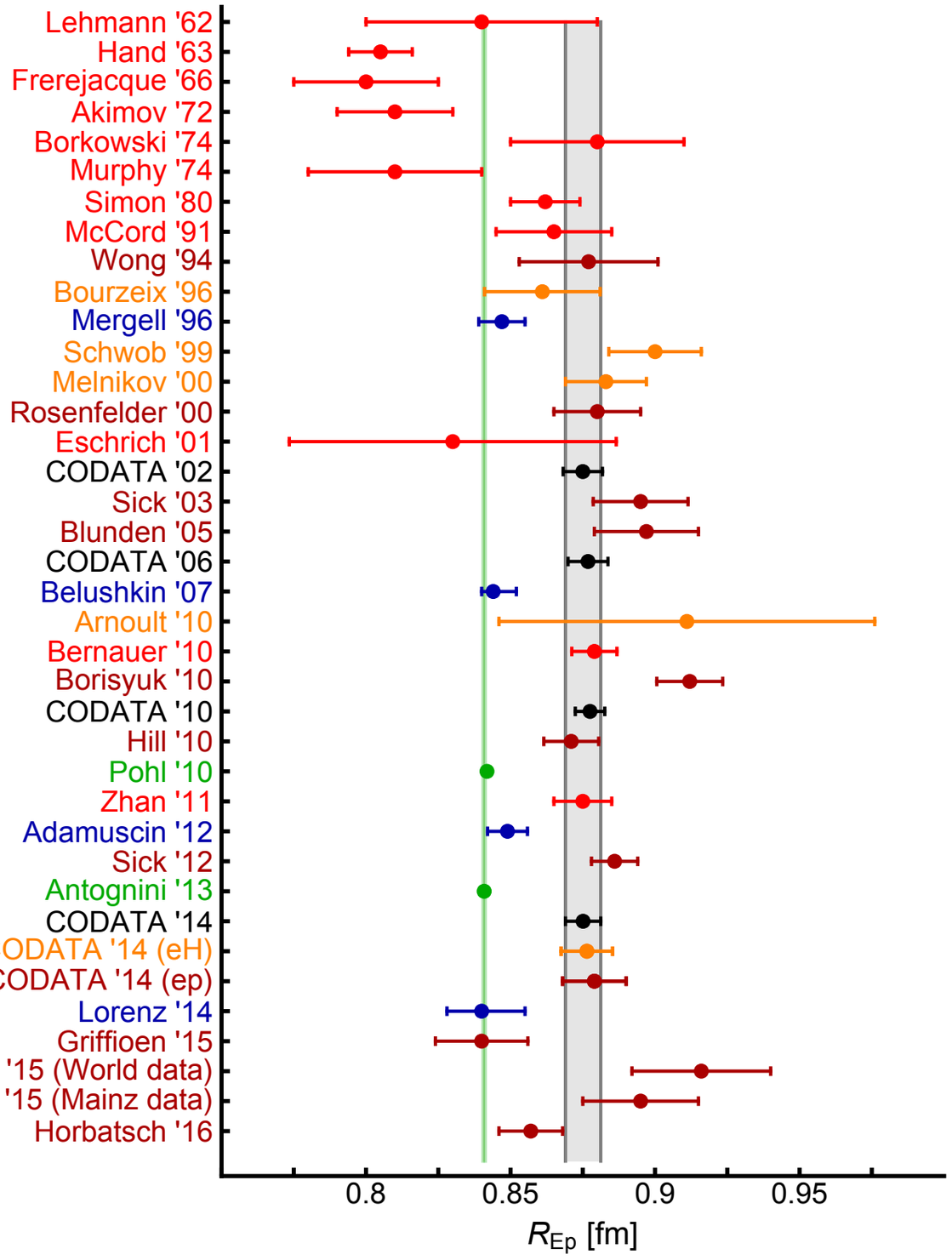

ep scattering, eH spectroscopy

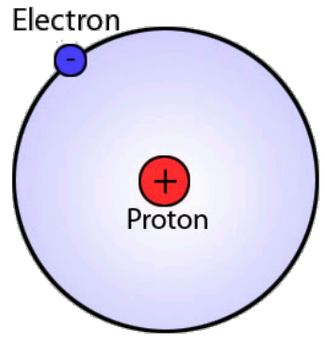

$$[R_{Ep}^{\text{CODATA 2014}} = 0.8751(61)\,\text{fm}]$$

[P. J. Mohr, et al., Rev. Mod. Phys. **84**, 1527 (2012).

5.6 σ discrepancy

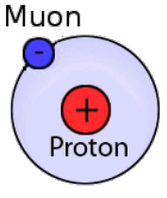

$$[R_{Ep}^{\mu\text{H}} = 0.84087(39)\,\text{fm}]$$

R. Pohl, A. Antognini et al., Nature **466**, 213 (2010)
A. Antognini et al., Science **339**, 417 (2013)

μH spectroscopy

LATEST NEWS

- Extraction of the proton radius from a new measurement of the hydrogen Lamb shift agrees with the value from the muonic-hydrogen Lamb shift

Bezginov et al., Science 365, 1007–1012 (2019).

ATOMIC PHYSICS

A measurement of the atomic hydrogen Lamb shift and the proton charge radius

N. Bezginov[1], T. Valdez[1], M. Horbatsch[1], A. Marsman[1], A. C. Vutha[2], E. A. Hessels[1]*

The surprising discrepancy between results from different methods for measuring the proton charge radius is referred to as the proton radius puzzle. In particular, measurements using electrons seem to lead to a different radius compared with those using muons. Here, a direct measurement of the $n = 2$ Lamb shift of atomic hydrogen is presented. Our measurement determines the proton radius to be $r_p = 0.833$ femtometers, with an uncertainty of ±0.010 femtometers. This electron-based measurement of r_p agrees with that obtained from the analogous muon-based Lamb shift measurement but is not consistent with the larger radius that was obtained from the averaging of previous electron-based measurements.

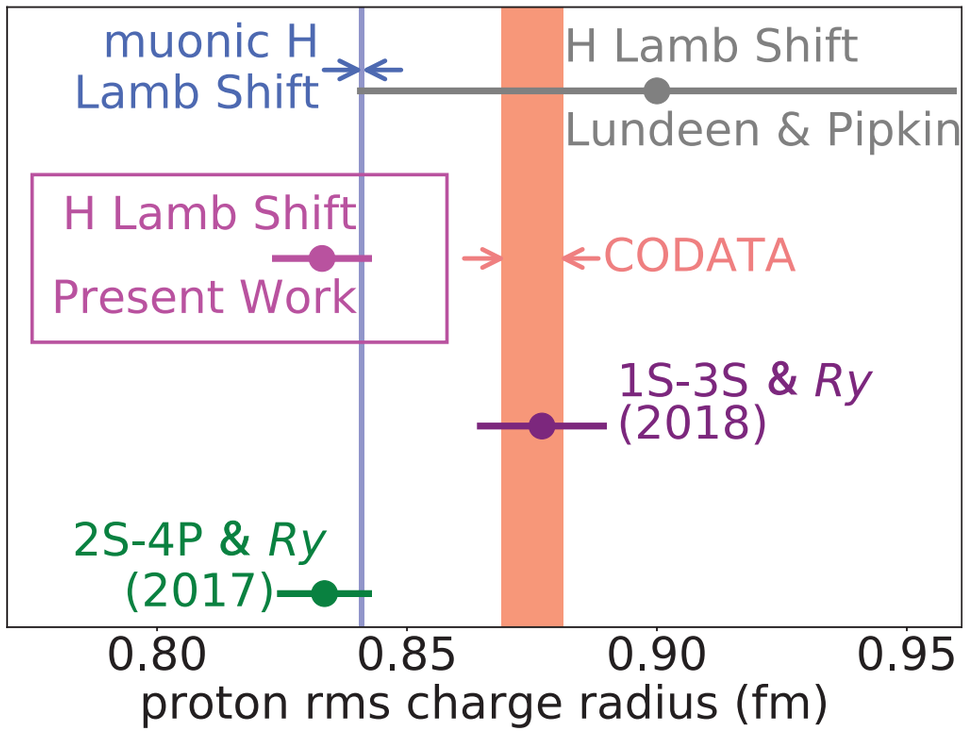

Fig. 5. Summary of proton radius data. Shown are values for the proton RMS charge radius from our measurement, muonic hydrogen, CODATA 2014, and the measurements of Beyer *et al*. (*18*) and Fleurbaey *et al*. (*19*) combined with that of Parthey *et al*. (*20*). Also shown in gray is the value from Lundeen and Pipkin (*6*, *16*).

POSSIBLE EXPLANATIONS

Why do we observe different radii ?

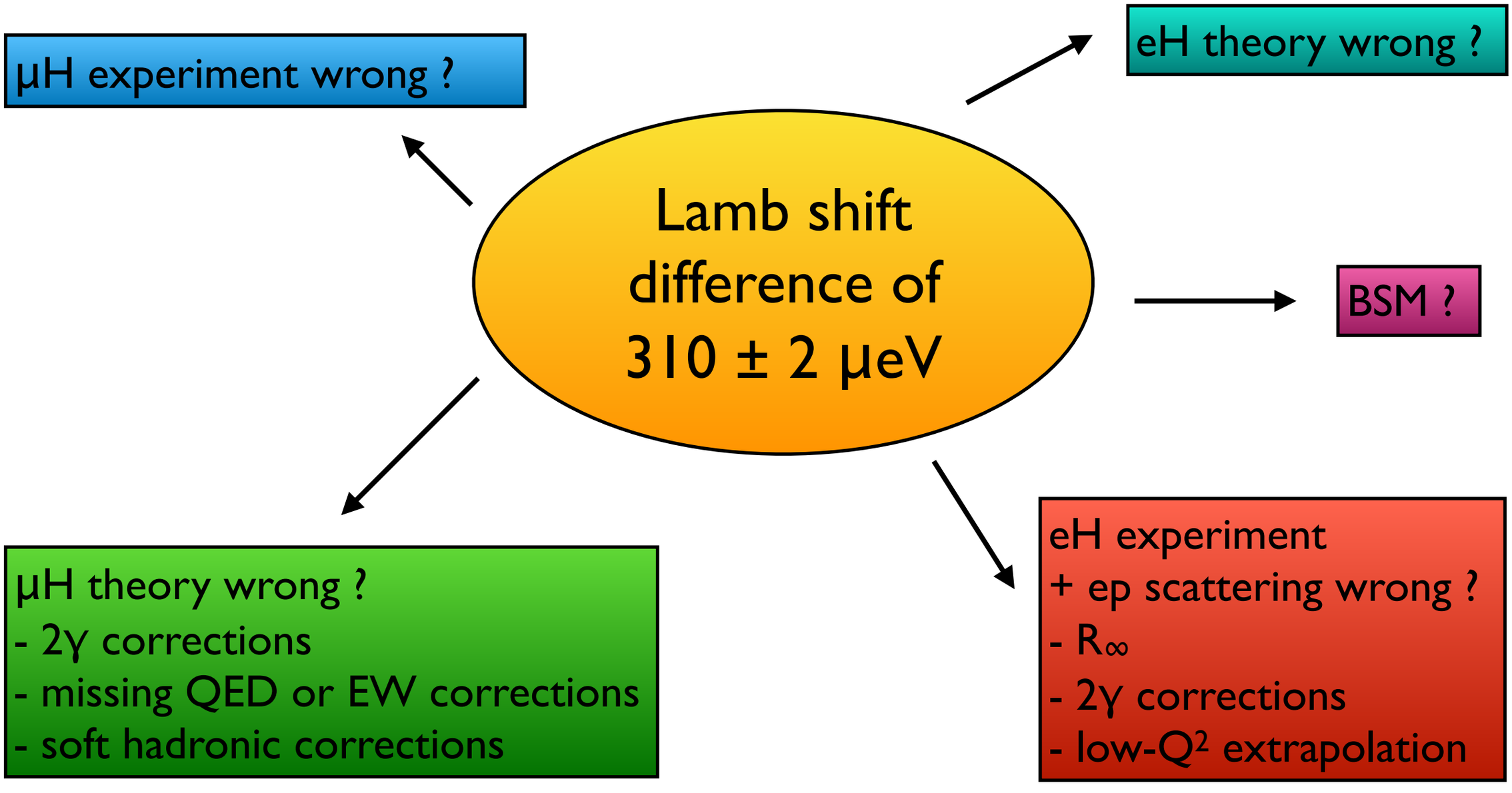

PROTON FORM FACTORS

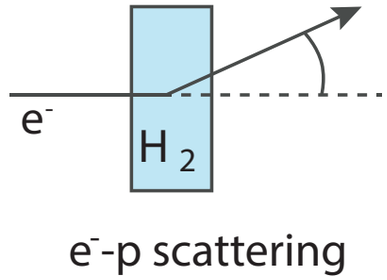

e-p scattering

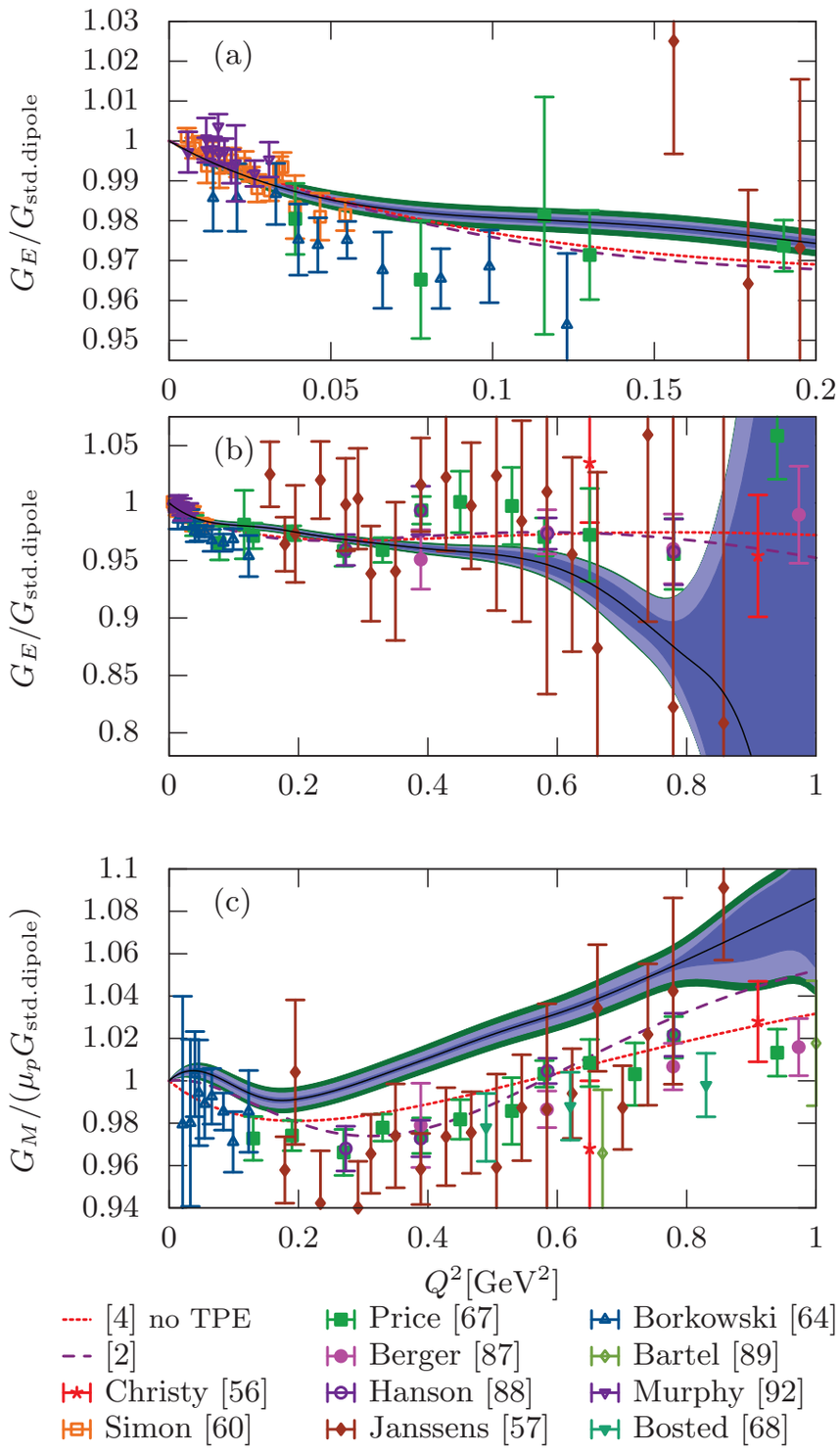

J. C. Bernauer *et al.*, Phys. Rev. C **90**, 015206 (2014)

- Form factors (FF): Fourier transforms of charge and magnetization distributions:

$$\rho(r) = \int \frac{\mathrm{d}\boldsymbol{q}}{(2\pi)^3} G(\boldsymbol{q}^2) e^{-i\boldsymbol{q}\boldsymbol{r}}$$

- Root-mean-square (rms) charge radius:

$$R_E = \sqrt{\langle r^2 \rangle_E}$$

$$\langle r^2 \rangle_E \equiv \int \mathrm{d}\boldsymbol{r}\, r^2\, \rho_E(\boldsymbol{r}) = -6 \frac{\mathrm{d}}{\mathrm{d}Q^2} G_E(Q^2)\Big|_{Q^2=0}$$

- Extraction of the proton charge radius from ep scattering requires extrapolation of FF data to zero momentum transfer

ANALYSING ELECTRON SCATTERING DATA

Avoiding common pitfalls and misconceptions in extractions of the proton radius

Jan C. Bernauer[1,*] and Michael O. Distler[2,†]

[1] *Laboratory for Nuclear Science, MIT, Cambridge, Massachusetts 02139, USA*
[2] *Institut für Kernphysik, Johannes-Gutenberg-Universität Mainz, D-55128 Mainz, Germany*

In a series of recent publications, different authors produce a wide range of electron radii when reanalyzing electron proton scattering data. In the light of the proton radius puzzle, this is a most unfortunate situation. However, we find flaws in most analyses that result in radii around 0.84 fm. In this paper, we explain our reasoning and try to illustrate the most common pitfalls.

How Variation in Analytic Choices Can Affect Normalization Parameters and Proton Radius Extractions From Electron Scattering Data

Douglas W. Higinbotham[1] and Randall E. McClellan[1]

[1] *Jefferson Lab, Newport News, VA 23606*

In order to make use of prior knowledge, such as analytic behavior or a known value at a kinematic endpoint, regressions often make use of floating normalization parameters to allow the fit to shift the data to the known physical limit. As there is often no unique way to make use of this prior knowledge or apply these shifts, different analysis choices can lead to very different conclusions from the same set of data. In this work, we use the Mainz elastic data set with its 1422 cross section points and 31 normalization parameters to illustrate how a single difference in a subjective analysis decision can dramatically affect the results.

The Proton Radius from Electron Scattering Data

Douglas W. Higinbotham,[1] Al Amin Kabir,[2] Vincent Lin,[1,3] David Meekins,[1] Blaine Norum,[4] and Brad Sawatzky[1]

[1] *Jefferson Lab, 12000 Jefferson Avenue, Newport News, Virginia 23606 USA*
[2] *Kent State University, 800 E. Summit St., Kent State, Ohio, 44240 USA*
[3] *Western Branch High School, 1968 Bruin Place, Chesapeake, VA 23321 USA*
[4] *University of Virginia, Charlottesville, Virginia 22904 USA*

Conclusions: Rigorous applications of stepwise regression techniques and multivariate error estimates result in the extraction of a proton charge radius that is consistent with the muonic hydrogen result of 0.84 fm; either from linear extrapolation of the extreme low-Q^2 data or by use of the Padé approximant for extrapolation using a larger range of data. Thus, based on a purely statistical analysis of electron scattering data, we conclude that the electron scattering result and the muonic hydrogen result are consistent. It is the atomic hydrogen results that are the outliers.

Robust extraction of the proton charge radius from electron-proton scattering data

Xuefei Yan,[1,2,*] Douglas W. Higinbotham,[3] Dipangkar Dutta,[4] Haiyan Gao,[1,2,5] Ashot Gasparian,[6] Mahbub A. Khandaker,[7] Nilanga Liyanage,[8] Eugene Pasyuk,[3] Chao Peng,[1,2] and Weizhi Xiong[1,2]

[1] *Duke University, Durham, North Carolina 27708, USA*
[2] *Triangle Universities Nuclear Laboratory, Durham, North Carolina 27708, USA*
[3] *Thomas Jefferson National Accelerator Facility, 12000 Jefferson Avenue, Newport News, Virginia 23606, USA*
[4] *Mississippi State University, Mississippi State 39762, USA*
[5] *Duke Kunshan University, Jiangsu 215316, China*
[6] *North Carolina A&T State University, Greensboro, North Carolina 27411, USA*
[7] *Idaho State University, Idaho 83209, USA*
[8] *University of Virginia, Charlottesville, VA 22904, USA*

Proton root-mean-square radii and electron scattering

Ingo Sick* and Dirk Trautmann†

Departement Physik, Universität Basel, CH4056 Basel, Switzerland

(Received 13 November 2013; published 6 January 2014)

The standard procedure of extracting the proton root-mean-square radii from models for the Sachs form factors $G_e(q)$ and $G_m(q)$ fitted to elastic electron-proton scattering data is more uncertain than traditionally assumed. The extrapolation of $G(q)$, from the region $q_{\min} < q < q_{\max}$ covered by data to momentum transfer $q = 0$ where the rms radius is obtained, often depends on uncontrolled properties of the parametrization used. Only when ensuring that the corresponding densities have a physical behavior at large radii r can reliable rms radii be determined.

Ingo Sick

Importance of Tail of Proton Density

Or: How to Get the *rms*-Radius from (e, e) Data

Consistency of electron scattering data with a small proton radius

Keith Griffioen, Carl Carlson, and Sarah Maddox

Physics Department, College of William and Mary, Williamsburg, Virginia 23187, USA

(Received 26 October 2015; published 17 June 2016)

We determine the charge radius of the proton by analyzing the published low momentum transfer electron-proton scattering data from Mainz. We note that polynomial expansions of the form factor converge for momentum transfers squared below $4m_\pi^2$, where m_π is the pion mass. Expansions with enough terms to fit the data, but few enough not to overfit, yield proton radii smaller than the CODATA or Mainz values and in accord with the muonic atom results. We also comment on analyses using a wider range of data, and overall obtain a proton radius $R_E = 0.840(16)$ fm.

The proton charge radius extracted from the Initial State Radiation experiment at MAMI

M. Mihovilovič[a,b,c], P. Achenbach[c], T. Beranek[c], J. Beričič[b], J. C. Bernauer[d], R. Böhm[c], D. Bosnar[e], M. Cardinali[c], L. Correa[f], L. Debenjak[b], A. Denig[c], M. O. Distler[c], A. Esser[c], M. I. Ferretti Bondy[c], H. Fonvieille[f], J. M. Friedrich[g], I. Friščić[d], K. Griffioen[h], M. Hoek[c], S. Kegel[c], Y. Kohl[c], H. Merkel[c,*], D. G. Middleton[c], U. Müller[c], J. Pochodzalla[c], B. S. Schlimme[c], M. Schoth[c], F. Schulz[c], C. Sfienti[c], S. Širca[a,b], S. Štajner[b], M. Thiel[c], A. Tyukin[c], M. Vanderhaeghen[c], A. B. Weber[c]

[a] *Faculty of Mathematics and Physics, University of Ljubljana, SI-1000 Ljubljana, Slovenia*
[b] *Jožef Stefan Institute, SI-1000 Ljubljana, Slovenia*
[c] *Institut für Kernphysik, Johannes Gutenberg-Universität Mainz, DE-55128 Mainz, Germany*
[d] *Massachusetts Institute of Technology, Cambridge, MA 02139, USA*
[e] *Department of Physics, Faculty of Science, University of Zagreb, HR-10002 Zagreb, Croatia*
[f] *Université Clermont Auvergne, CNRS/IN2P3, LPC, BP 10448, F-63000 Clermont-Ferrand, France*
[g] *Technische Universität München, Physik Department, 85748 Garching, Germany*
[h] *College of William and Mary, Williamsburg, VA 23187, USA*

ep scattering talks by Douglas, Haiyan, Jan, Miha and Ulrich

FH and V. Pascalutsa, Phys. Lett. B 797 (2019)

Lower bound on the proton charge radius from electron scattering data

Franziska Hagelstein [a], Vladimir Pascalutsa [b,*]

[a] Albert Einstein Center for Fundamental Physics, Institute for Theoretical Physics, University of Bern, Sidlerstrasse 5, CH-3012 Bern, Switzerland
[b] Institut für Kernphysik and Cluster of Excellence PRISMA, Johannes Gutenberg Universität Mainz, D-55128 Mainz, Germany

ARTICLE INFO

Article history:
Received 1 January 2019
Received in revised form 18 July 2019
Accepted 30 July 2019
Available online 1 August 2019
Editor: V. Metag

Keywords:
Charge radius
Proton size
Form factors
Charge distribution
Electron scattering

ABSTRACT

The proton charge-radius determinations from the electromagnetic form-factor measurements in electron-proton (ep) scattering require an extrapolation to zero momentum transfer ($Q^2 = 0$) which is prone to model-dependent assumptions. We show that the data at finite momentum transfer can be used to establish a rigorous lower bound on the proton charge radius, while bypassing the model-dependent assumptions that go into the fitting and extrapolation of the ep data. The near-future precise ep experiments at very low Q^2, such as PRad, are expected to set a stringent lower bound on the proton radius.

Disclaimer: "For illustrative purposes, we have made a tentative determination of the lower bound on the proton charge radius from the available data in the region of Q^2 below 0.02 GeV^2. … our uncertainty estimate is only indicative and should be taken with caution. The treatment of systematic errors, most notably the normalization uncertainty, is rather involved in this particular experiment and entangled with the radius extraction."

LOW-Q SCATTERING DATA

- Fitting and extrapolating form factor data is not easy:

LOW-Q SCATTERING DATA

- Fitting and extrapolating form factor data is not easy:
  - Difficult to quantify the extend to which the slope at zero momentum transfer is determined by the behavior at finite Q

LOW-Q SCATTERING DATA

- Fitting and extrapolating form factor data is not easy:
  - Difficult to quantify the extend to which the slope at zero momentum transfer is determined by the behavior at finite *Q*

Proton Electric Form Factor: G_E (Preliminary)

- Proton electric form factor: G_E vs. Q^2 from 2.2 and 1.1 GeV data

(G_M used from J.J Kelly, PRC 70 (2004) 068202)

- Systematic uncertainties shown as colored error bars.
- Preliminary G_E slop seems to favor smaller radius.

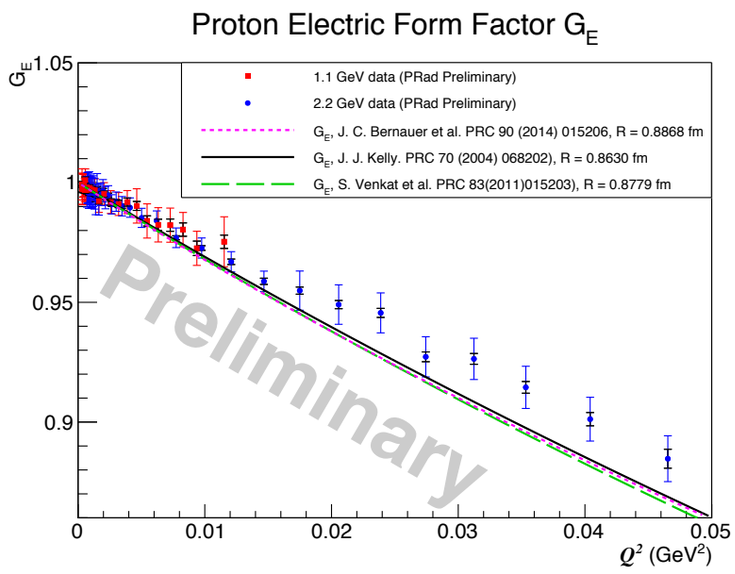

Proton Electric Form Factor: G_E (Preliminary)

- G_E vs. Q^2, from 2.2 and 1.1 GeV data

(G_M used from J.J Kelly, PRC 70 (2004) 068202)

- Q^2 range from 6×10^{-4} to 1.5×10^{-2} GeV^2 shown only.
- Systematic uncertainties shown as colored error bars
- Preliminary G_E slop seems to favor smaller radius.

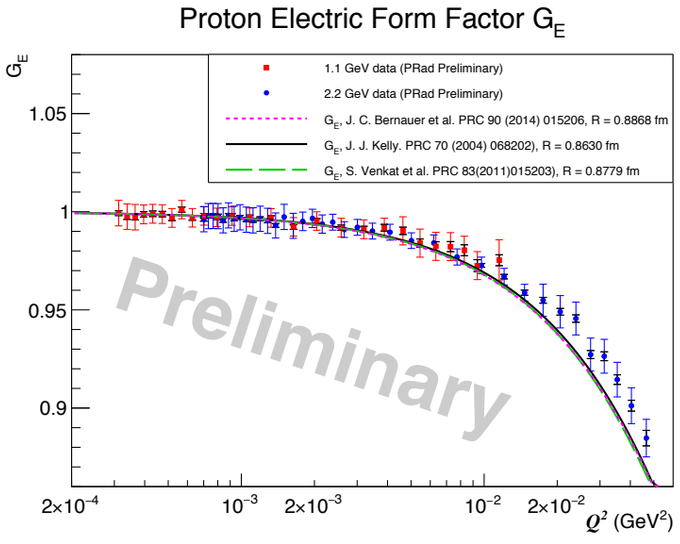

A. Gasparian, PRP 2018

LOW-Q SCATTERING DATA

- Fitting and extrapolating FF data is not easy:
  - Difficult to quantify the extend to which the slope at zero momentum transfer is determined by the behavior at finite *Q*

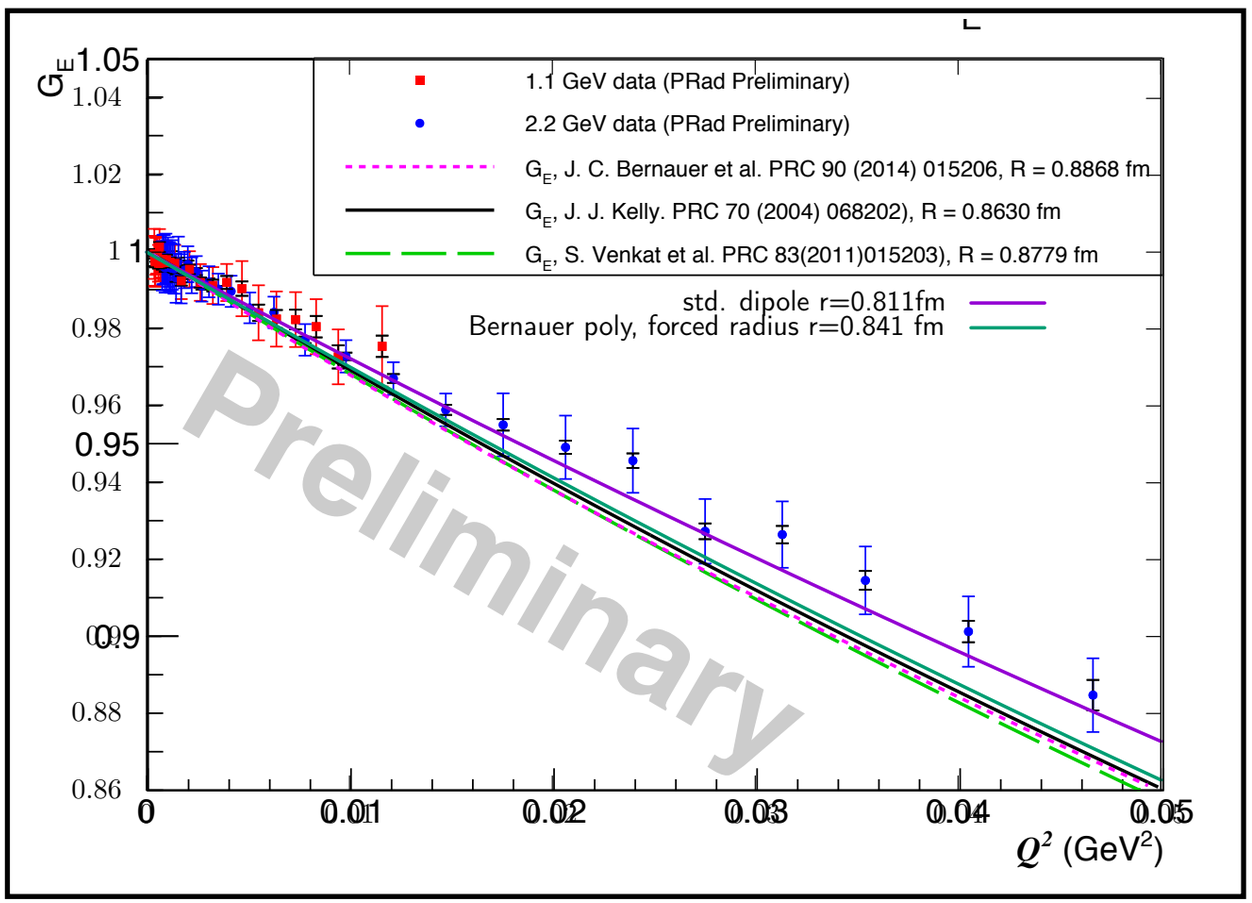

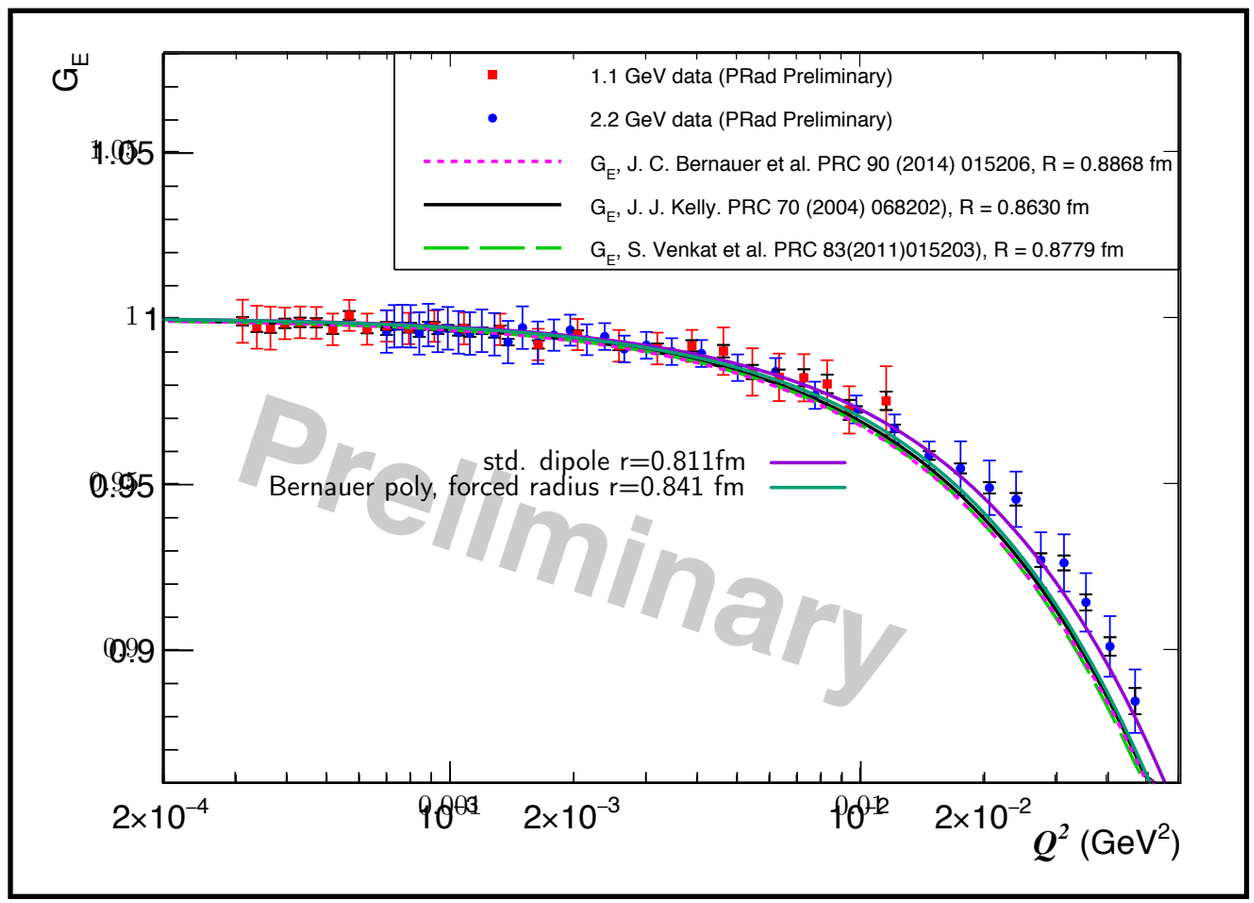

J. Bernauer, PRP 2018

LOW-Q SCATTERING DATA

- Fitting and extrapolating FF data is not easy:
  - Difficult to quantify the extend to which the slope at zero momentum transfer is determined by the behavior at finite *Q*
  - Also lattice QCD data at low Q is severely suffering from finite volume effects

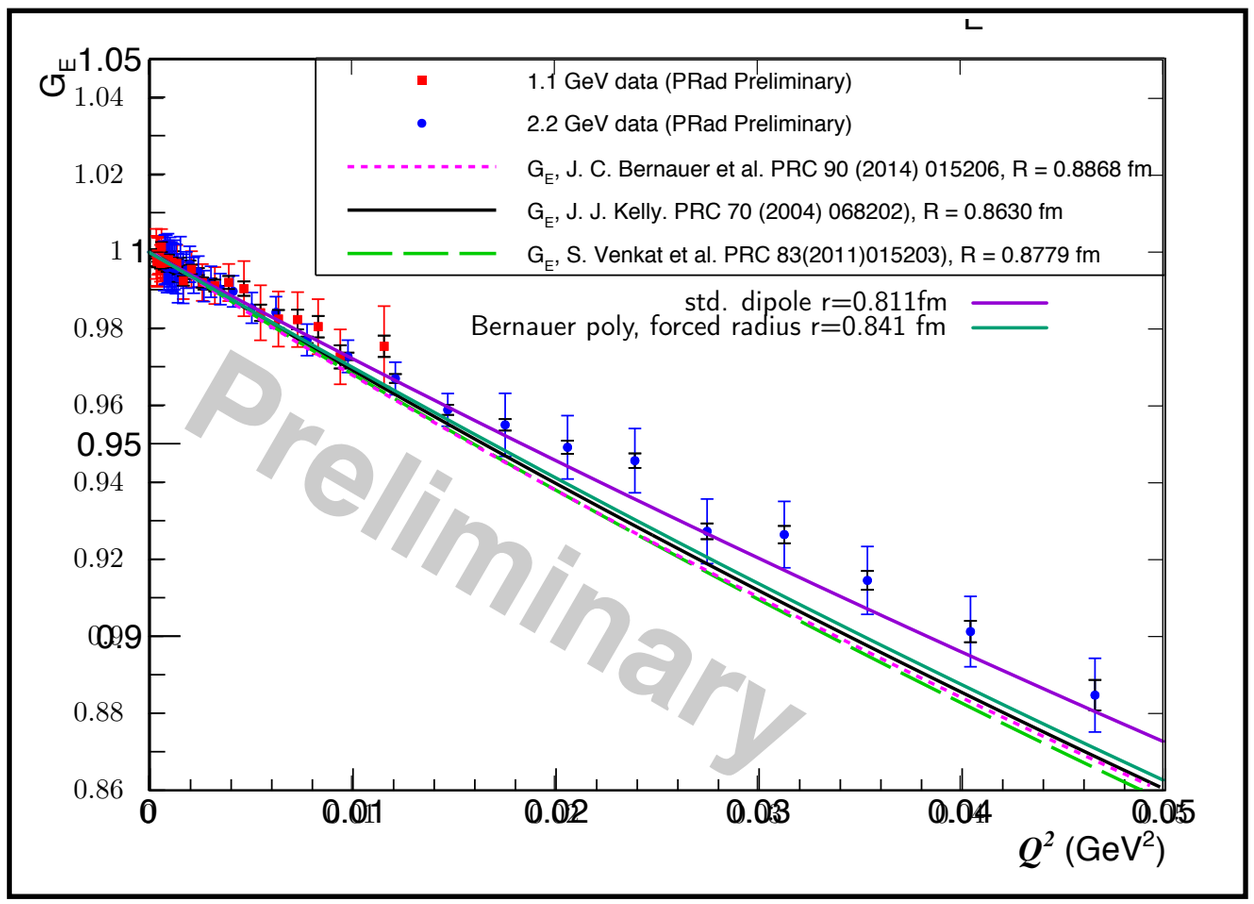

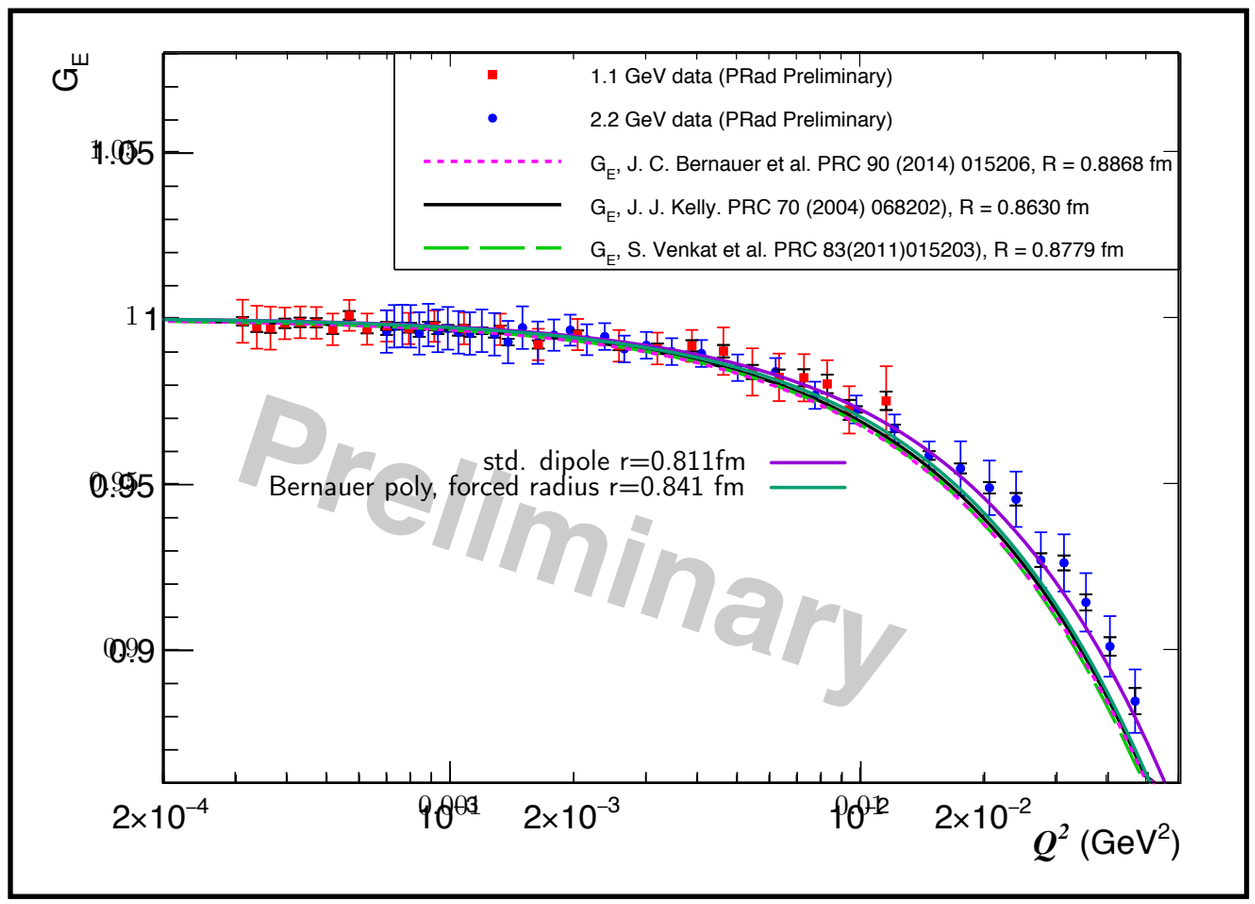

J. Bernauer, PRP 2018

LOWER BOUND ON CHARGE RADIUS

$$R_E^2(Q^2) = -\frac{6}{Q^2}\log G_E(Q^2) \xrightarrow{Q^2=0} R_E^2$$ is a lower bound $\boxed{R_E^2(Q^2) \leq R_E^2}$ for $Q^2 \geq 0$

- $R_E^2(Q^2)$ is monotonically increasing towards $Q^2=0$
- Lower bound follows from finite Q^2 data, no extrapolation of FF data required

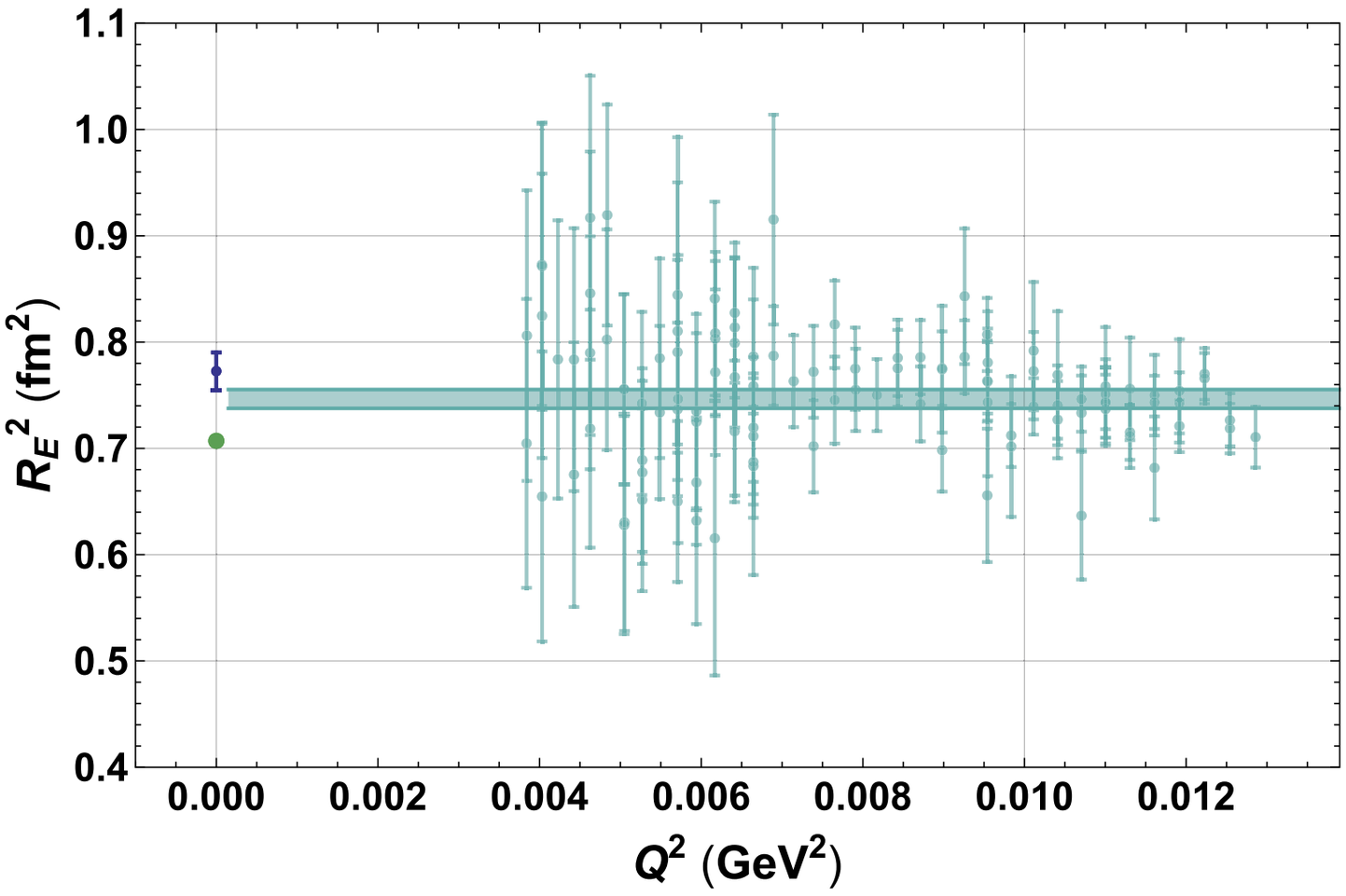

FH and V. Pascalutsa, Phys. Lett. B 797 (2019)

RMS CHARGE RADIUS

- RMS charge radius: $R_E^2 = -6 \left. \frac{\mathrm{d}\, G_E(Q^2)}{\mathrm{d}Q^2} \right|_{Q^2=0} = 4\pi \int_0^\infty \mathrm{d}r\, r^4\, \rho_E(r)$

RMS CHARGE RADIUS

- RMS charge radius: $R_E^2 = -6 \left. \frac{\mathrm{d}\, G_E(Q^2)}{\mathrm{d}Q^2} \right|_{Q^2=0} = 4\pi \int_0^\infty \mathrm{d}r\, r^4\, \rho_E(r)$

- $G_E(Q^2) = 4\pi \int_0^\infty \mathrm{d}r\, r^2\, j_0(Qr)\, \rho_E(r)$ with the spherically symmetric charge density $\rho_E(r)$ and the spherical Bessel function $j_0(x) = \frac{\sin x}{x}$

- $G_E(Q^2)$ and $\rho_E(r)$ are Lorentz-invariant quantities

RMS CHARGE RADIUS

- RMS charge radius: $R_E^2 = -6 \left. \frac{\mathrm{d}\, G_E(Q^2)}{\mathrm{d}Q^2} \right|_{Q^2=0} = 4\pi \int_0^\infty \mathrm{d}r\, r^4\, \rho_E(r)$

- $G_E(Q^2) = 4\pi \int_0^\infty \mathrm{d}r\, r^2\, j_0(Qr)\, \rho_E(r)$ with the spherically symmetric charge density $\rho_E(r)$ and the spherical Bessel function $j_0(x) = \frac{\sin x}{x}$
  - $G_E(Q^2)$ and $\rho_E(r)$ are Lorentz-invariant quantities

- Taylor expansion, $G_E(Q^2) = 1 - Q^2 \langle r^2 \rangle_E / 6 + Q^4 \langle r^4 \rangle_E / 120 + \ldots$, convergence radius is limited by the onset of the pion-production branch cut at $Q^2 \ll 4m_\pi^2 \sim 0.08\,\mathrm{GeV}^2$
  - Dispersive fits and z-expansion take singularities into account but have other limitations

DERIVATION OF THE LOWER BOUND

Lower-bound function: $R_E^2(Q^2) = -\frac{6}{Q^2}\log G_E(Q^2)$

DERIVATION OF THE LOWER BOUND

Lower-bound function: $R_E^2(Q^2) = -\frac{6}{Q^2}\log G_E(Q^2)$

- $R_E^2(Q^2) \geq 0$, since $G_E(Q^2) \leq 1$

DERIVATION OF THE LOWER BOUND

Lower-bound function: $R_E^2(Q^2) = -\frac{6}{Q^2}\log G_E(Q^2)$

- $R_E^2(Q^2) \geq 0$, since $G_E(Q^2) \leq 1$

Show that $G_E(Q^2) \leq 1$ for $Q^2 \geq 0$:

- $G_E(Q^2) = F_1(Q^2) - \frac{Q^2}{4M^2}F_2(Q^2)$
- $F_2(Q^2) \geq 0$ (empirically known, e.g., $F_2(0) = \kappa$)
- $F_1(Q^2) \leq 1$ follows from positive definiteness of the transverse charge density $\rho_\perp(b) \geq 0$ — since $F_1(0) - F_1(Q^2) = 2\pi\int_0^\infty \mathrm{d}b\, b\, \left[1 - J_0(Qb)\right]\, \rho_\perp(b) > 0$ with the cylindrical Bessel function $J_0(x) \leq 1$

DERIVATION OF THE LOWER BOUND

Lower-bound function: $R_E^2(Q^2) = -\frac{6}{Q^2}\log G_E(Q^2)$

- $R_E^2(Q^2) \geq 0$, since $G_E(Q^2) \leq 1$
- $R_E^2(Q^2)$ falls with increasing Q^2, if G_E falls not faster than by a power law

DERIVATION OF THE LOWER BOUND

Lower-bound function: $R_E^2(Q^2) = -\frac{6}{Q^2}\log G_E(Q^2)$

- $R_E^2(Q^2) \geq 0$, since $G_E(Q^2) \leq 1$
- $R_E^2(Q^2)$ falls with increasing Q^2, if G_E falls not faster than by a power law
- $R_E^2(Q^2)$ is monotonic in the space-like region

- Unsubtracted dispersion relation: $R_E^2(Q^2) = \frac{1}{\pi}\int_{4m_p i^2}^{\infty} \mathrm{d}t\, \frac{\mathrm{Im}\, R_E^2(t)}{t+Q^2}$, with

  $\mathrm{Im}R_E^2(t) = \frac{6\,\varphi_E(t)}{t}$ and $\varphi(t) \geq 0$ is the phase defined through

  $G_E(t) = |G_E(t)|\, e^{i\varphi(t)}$

DERIVATION OF THE LOWER BOUND

Lower-bound function: $R_E^2(Q^2) = -\frac{6}{Q^2}\log G_E(Q^2)$

- $R_E^2(Q^2) \geq 0$, since $G_E(Q^2) \leq 1$
- $R_E^2(Q^2)$ falls with increasing Q^2, if G_E falls not faster than by a power law
- $R_E^2(Q^2)$ is monotonic in the space-like region

- Unsubtracted dispersion relation: $R_E^2(Q^2) = \frac{1}{\pi}\int_{4m_p i^2}^{\infty} \mathrm{d}t\, \frac{\mathrm{Im}\, R_E^2(t)}{t+Q^2}$, with

  $\mathrm{Im}R_E^2(t) = \frac{6\,\varphi_E(t)}{t}$ and $\varphi(t) \geq 0$ is the phase defined through

  $G_E(t) = |G_E(t)|\, e^{i\varphi(t)}$

- Limit equals the proton radius: $\lim_{Q^2\to 0} R_E^2(Q^2) = -6\,\frac{G_E'(Q^2)}{G_E(Q^2)}\Big|_{Q^2=0} = R_E^2$

EVALUATION OF THE LOWER BOUND

Lower-bound function: $R_E^2(Q^2) = -\frac{6}{Q^2}\log G_E(Q^2)$

EVALUATION OF THE LOWER BOUND

Lower-bound function: $R_E^2(Q^2) = -\frac{6}{Q^2}\log G_E(Q^2)$

- Each data point gives a lower bound — statistical average is used for a more accurate value

EVALUATION OF THE LOWER BOUND

Lower-bound function: $R_E^2(Q^2) = -\frac{6}{Q^2}\log G_E(Q^2)$

- Each data point gives a lower bound — statistical average is used for a more accurate value
- Data below $Q^2 < 0.02\,\mathrm{GeV}^2$ away from pion-production branch cut

EVALUATION OF THE LOWER BOUND

Lower-bound function: $R_E^2(Q^2) = -\frac{6}{Q^2}\log G_E(Q^2)$

- Each data point gives a lower bound — statistical average is used for a more accurate value
- Data below $Q^2 < 0.02\,\mathrm{GeV}^2$ away from pion-production branch cut
- Lower cut at $Q_0^2 \sim 0.01\,\mathrm{GeV}^2$

EVALUATION OF THE LOWER BOUND

Lower-bound function: $R_E^2(Q^2) = -\frac{6}{Q^2}\log G_E(Q^2)$

- Each data point gives a lower bound — statistical average is used for a more accurate value
- Data below $Q^2 < 0.02\,\mathrm{GeV}^2$ away from pion-production branch cut
- Lower cut at $Q_0^2 \sim 0.01\,\mathrm{GeV}^2$
  - Assume a small normalization error ϵ, such that $G_E^{(\mathrm{exp})} = (1+\epsilon)\,G_E$
  - Lower-bound function observed in experiment: $R_E^{2(\mathrm{exp})}(Q^2) = R_E^2(Q^2) - \frac{6}{Q^2}\ln(1+\epsilon)$
    - Lower bound is preserved, $R_E^{2(\mathrm{exp})}(Q^2) \leq R_E^2(Q^2)$, if $\epsilon > 0$
    - Lower bound is violated, $R_E^{2(\mathrm{exp})}(Q^2) \not\leq R_E^2(Q^2)$ for $Q^2 < Q_0^2$, if $\epsilon < 0$
  - Estimate lower cut with $\epsilon = -0.001$ and $Q_0^2 = \sqrt{\frac{-6\ln(1+\epsilon)}{\langle r^4\rangle_E/20 - R_E^4/12}}$

NORMALIZATION UNCERTAINTY

- Normalization of FF data is in general more complicated:
  - MAMI data have 31 (fitted) normalization parameters
  - Different fit of normalization parameters can generate a shift of the data

NORMALIZATION UNCERTAINTY

- Normalization of FF data is in general more complicated:
  - MAMI data have 31 (fitted) normalization parameters
  - Different fit of normalization parameters can generate a shift of the data
- Assume a highly-correlated systematic normalization uncertainty:
  - Averaging a dataset $A_i \pm \sigma_i \pm \Delta$ with correlated systematic error Δ, is equivalent to averaging the dataset $A_i \pm \sigma_i'$ with $\sigma_i' = \sigma_i \left(1 + \Delta^2 \sum_j 1/\sigma_j^2 \right)^{1/2}$
  - $\Delta = 0.001$ leads to $\sigma_i' \sim 4.5\, \sigma_i$

NORMALIZATION UNCERTAINTY

- Normalization of FF data is in general more complicated:
  - MAMI data have 31 (fitted) normalization parameters
  - Different fit of normalization parameters can generate a shift of the data
- Assume a highly-correlated systematic normalization uncertainty:
  - Averaging a dataset $A_i \pm \sigma_i \pm \Delta$ with correlated systematic error Δ, is equivalent to averaging the dataset $A_i \pm \sigma_i'$ with $\sigma_i' = \sigma_i \left(1 + \Delta^2 \sum_j 1/\sigma_j^2 \right)^{1/2}$
  - $\Delta = 0.001$ leads to $\sigma_i' \sim 4.5\, \sigma_i$
- Alternatively one can study subsets where the normalization is an overall factor

NORMALIZATION UNCERTAINTY

- Normalization of FF data is in general more complicated:
  - MAMI data have 31 (fitted) normalization parameters
  - Different fit of normalization parameters can generate a shift of the data
- Assume a highly-correlated systematic normalization uncertainty:
  - Averaging a dataset $A_i \pm \sigma_i \pm \Delta$ with correlated systematic error Δ, is equivalent to averaging the dataset $A_i \pm \sigma_i'$ with $\sigma_i' = \sigma_i \left(1 + \Delta^2 \sum_j 1/\sigma_j^2 \right)^{1/2}$
  - $\Delta = 0.001$ leads to $\sigma_i' \sim 4.5\, \sigma_i$
- Alternatively one can study subsets where the normalization is an overall factor
- Proper error evaluation should use the covariance matrix established in the experimental analysis

LOWER BOUND ON CHARGE RADIUS

$$R_E^2(Q^2) = -\frac{6}{Q^2}\log G_E(Q^2) \xrightarrow{Q^2=0} R_E^2$$ is a lower bound $\boxed{R_E^2(Q^2) \leq R_E^2}$ for $Q^2 \geq 0$

- $R_E^2(Q^2)$ is monotonically increasing towards $Q^2=0$
- Lower bound follows from finite Q^2 data, no extrapolation / model dependence

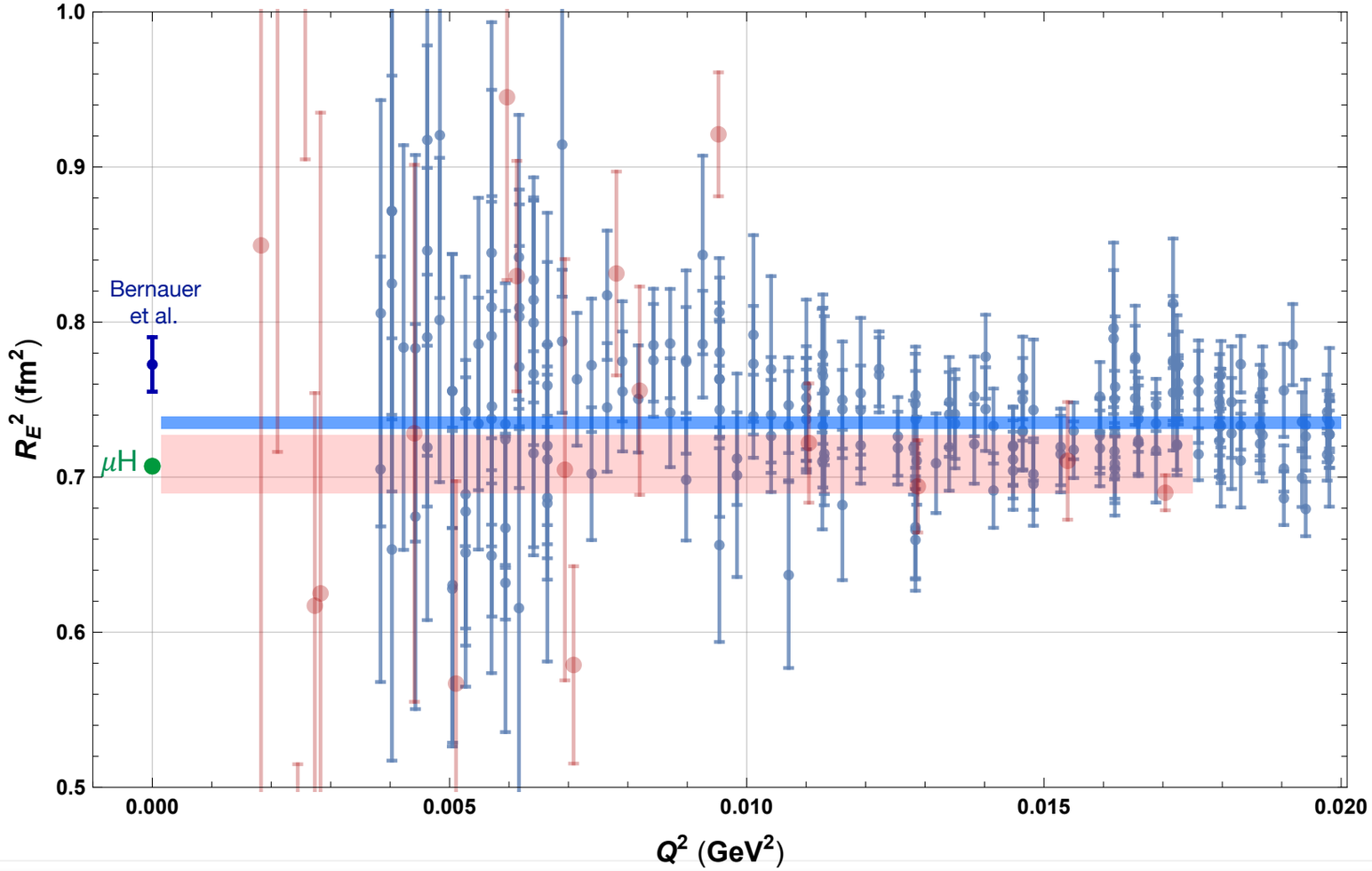

Data points from A1 Coll.:

Bernauer et al (2010)

Mihovilovic et al (2017)

Dataset		Average $\sqrt{R_E^2(Q^2)}$
Bernauer et al. [4]	$Q^2 < 0.02$ GeV^2	0.857 ± 0.010
	subset "1:3"	0.864 ± 0.016
Mihovilović et al. [30]	all data	0.842 ± 0.011

FH and V. Pascalutsa, Phys. Lett. B 797 (2019)

VARIOUS PROTON RADIUS EXTRACTIONS

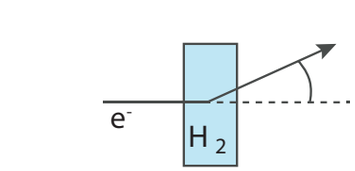

e⁻-p scattering

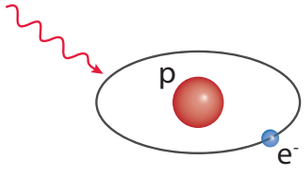

H spectroscopy

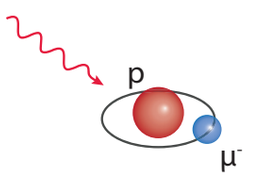

μp spectroscopy

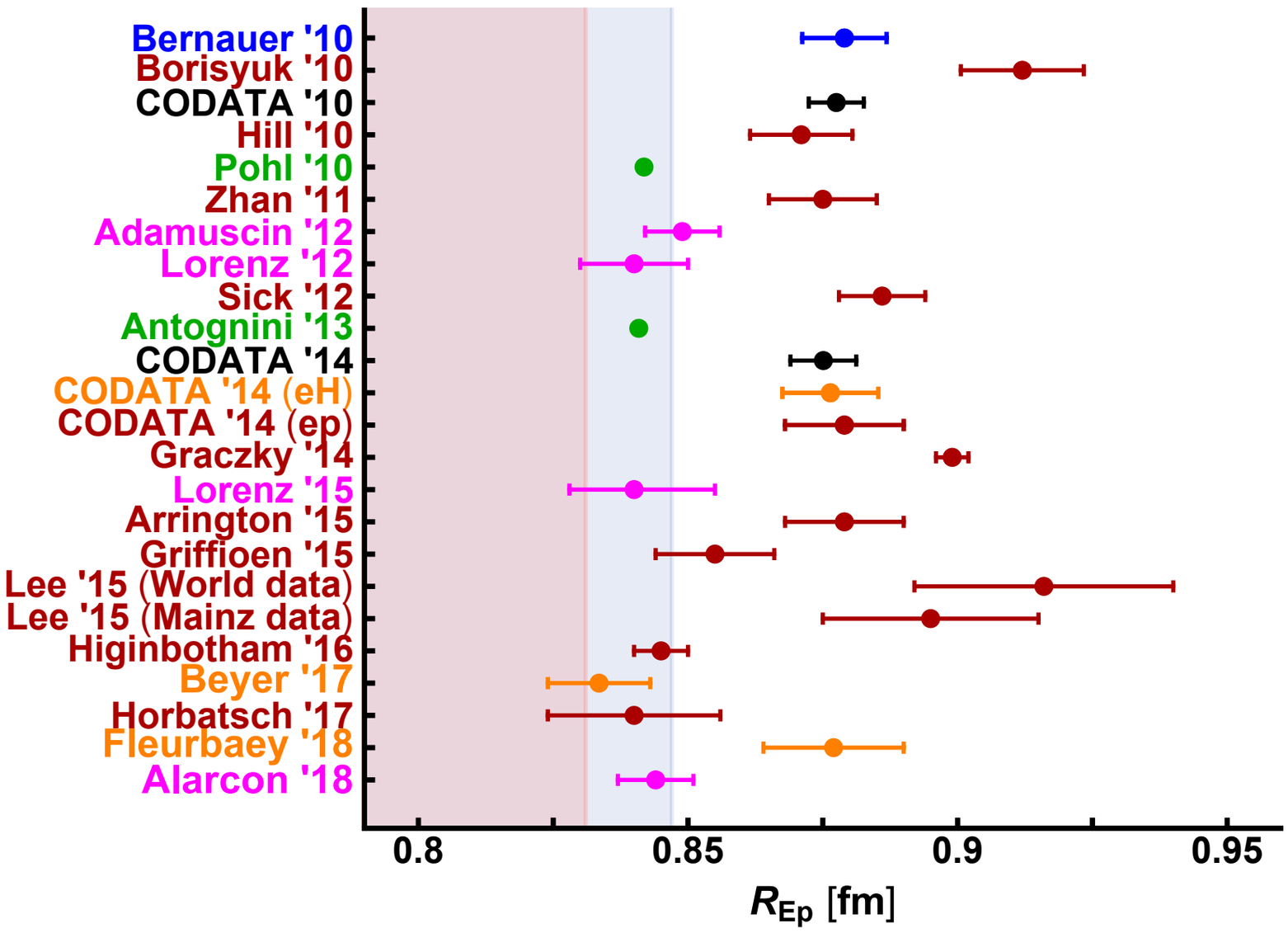

- Forthcoming results of the PRad experiment might allow for a better determination of the lower bound on the proton charge radius
  - $Q^2 > 2 \times 10^{-4}\,\mathrm{GeV}^2$
  - simultaneous measurement of the Møller scattering gives precise normalization

FH and V. Pascalutsa, Phys. Lett. B 797 (2019)

MITP - PROTON RADIUS 2018

mitp **Mainz Institute for Theoretical Physics**

SCIENTIFIC PROGRAMS

Probing Physics Beyond the SM with Precision
Ansgar Denner **U Würzburg**, Stefan Dittmaier **U Freiburg**, Tilman Plehn **Heidelberg U**
February 26 - March 9, 2018

Bridging the Standard Model to New Physics with the Parity Violation Program at MESA
Jens Erler **UNAM**, Mikhail Gorshteyn, Hubert Spiesberger **JGU**
April 23 - May 4, 2018

Modern Techniques for CFT and AdS
Bartlomiej Czech **IAS Princeton**, Michal P. Heller **MPI for Gravitational Physics**, Alessandro Vichi **EPFL**
May 22 - 30, 2018

The Dawn of Gravitational Wave Science
Luis Lehner **Perimeter Inst.**, Rafael A. Porto **ICTP-SAIFR**, Riccardo Sturani **IIP Natal**, Salvatore Vitale **MIT**
June 4 - 15, 2018

The Future of BSM Physics
Gian Giudice **CERN**, Giulia Ricciardi **U Naples Federico II**, Tobias Hurth, Joachim Kopp, Matthias Neubert **JGU**
June 4 - 15, 2018, Capri, Italy

TOPICAL WORKSHOPS

The Evaluation of the Leading Hadronic Contribution to the Muon Anomalous Magnetic Moment
Carlo Carloni Calame **INFN Pavia**, Massimo Passera **INFN Padua**, Luca Trentadue **U Parma**, Graziano Venanzoni **INFN Pisa**
February 19 - 23, 2018

Applied Newton-Cartan Geometry
Eric Bergshoeff **U Groningen**, Niels Obers **NBI Copenhagen**, Dam Thanh Son **U Chicago**
March 12 - 16, 2018

Challenges in Semileptonic B Decays
Paolo Gambino **U Turin**, Andreas Kronfeld **Fermilab**, Marcello Rotondo **INFN-LNF Frascati**, Christoph Schwanda **ÖAW Vienna**
April 9 - 13, 2018

Tensions in the LCDM Paradigm
Cora Dvorkin **Harvard**, Silvia Galli **IAP Paris**, Fabio Iocco **ICTP-SAIFR**, Federico Marinacci **MIT**
May 14 - 18, 2018

The Proton Radius Puzzle and Beyond
Richard Hill **U Kentucky / Fermilab**, Gil Paz **Wayne State U**, Randolf Pohl **JGU**
July 23 - 27, 2018

Conference proceedings / white paper in preparation!

Nuclear structure effects in light muonic atoms

Carl E. Carlson,[1] Franziska Hagelstein,[2] Oscar J. Hernandez,[3,4,5] Antonio Pineda,[6] Oleksandr Tomalak,[3,7,8] and Krzysztof Pachucki[9]

[1]*College of William and Mary, Physics Department, Williamsburg, Virginia 23187, USA*
[2]*Albert Einstein Center for Fundamental Physics, Institute for Theoretical Physics, University of Bern, CH-3012 Bern, Switzerland*
[3]*Institut für Kernphysik and PRISMA Cluster of Excellence, Johannes Gutenberg Universität, Mainz, D-55099, Germany*
[4]*Department of Physics and Astronomy, University of British Columbia, Vancouver, BC, V6T 1Z4, Canada*
[5]*TRIUMF, 4004 Wesbrook Mall, Vancouver, BC V6T 2A3, Canada*
[6]*Grup de Física Teòrica, Dept. Física and IFAE-BIST, Universitat Autònoma de Barcelona, E-08193 Bellaterra (Barcelona), Spain*
[7]*Department of Physics and Astronomy, University of Kentucky, Lexington, KY 40506, USA*
[8]*Fermilab, Batavia, IL 60510, USA*
[9]*Faculty of Physics, University of Warsaw, Pasteura 5, 02-093 Warsaw, Poland*

FINITE-SIZE EFFECTS

Why muonic atoms ?

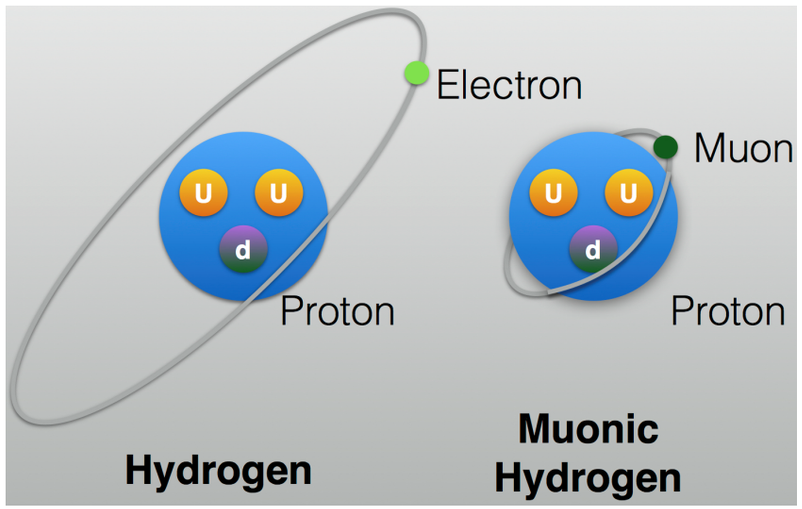

- **Lamb shift:**

wave function at the origin

$$\Delta E_{nl}(\mathrm{LO+NLO}) = \delta_{l0}\,\frac{2\pi Z\alpha}{3}\,\frac{1}{\pi(an)^3}\left[R_E^2 - \frac{Z\alpha m_r}{2}R_{E(2)}^3\right]$$

NLO becomes appreciable in μH

- **HFS:**

$$\Delta E_{nS}(\mathrm{LO+NLO}) = E_F(nS)\,[1 - 2\,Z\alpha m_r\,R_Z]$$

Fermi - Energy:

$$E_F(nS) = \frac{8}{3}\frac{Z\alpha}{a^3}\frac{1+\kappa}{mM}\frac{1}{n^3}$$

with Bohr radius $a = 1/(Z\alpha m_r)$

THEORY OF μH LAMB SHIFT

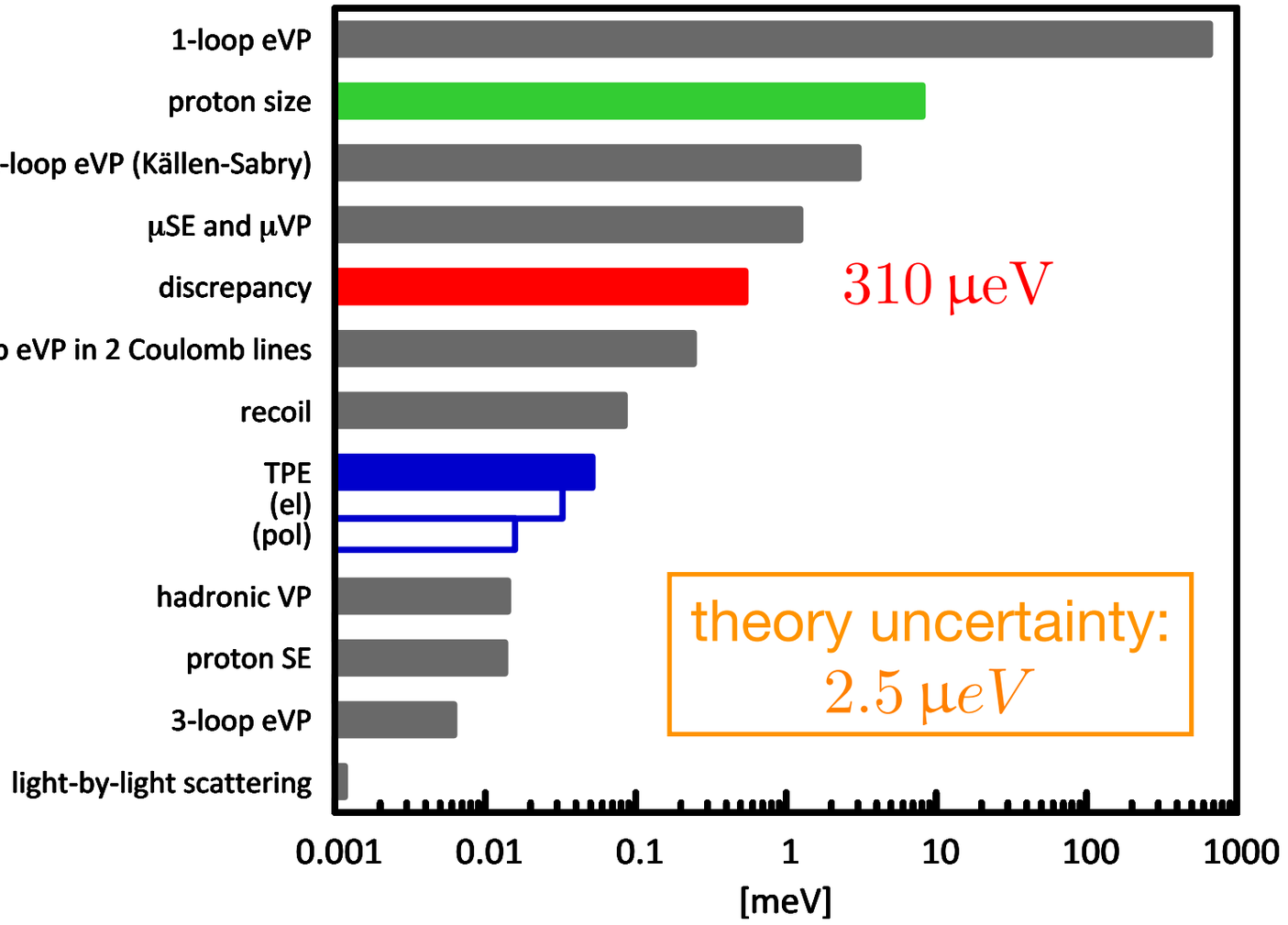

$$E_{\rm LS}^{\mu\rm H\ th.} = 206.0336(15) - 5.2275(10)\left(\frac{R_E}{\rm fm}\right)^2 + E_{\rm LS}^{2\gamma} \qquad \text{[values in meV]}$$

$$E_{\rm LS} = -\frac{\alpha}{12a^3}R_E^2 + \mathcal{O}(\alpha^5)$$

THEORY OF μH LAMB SHIFT

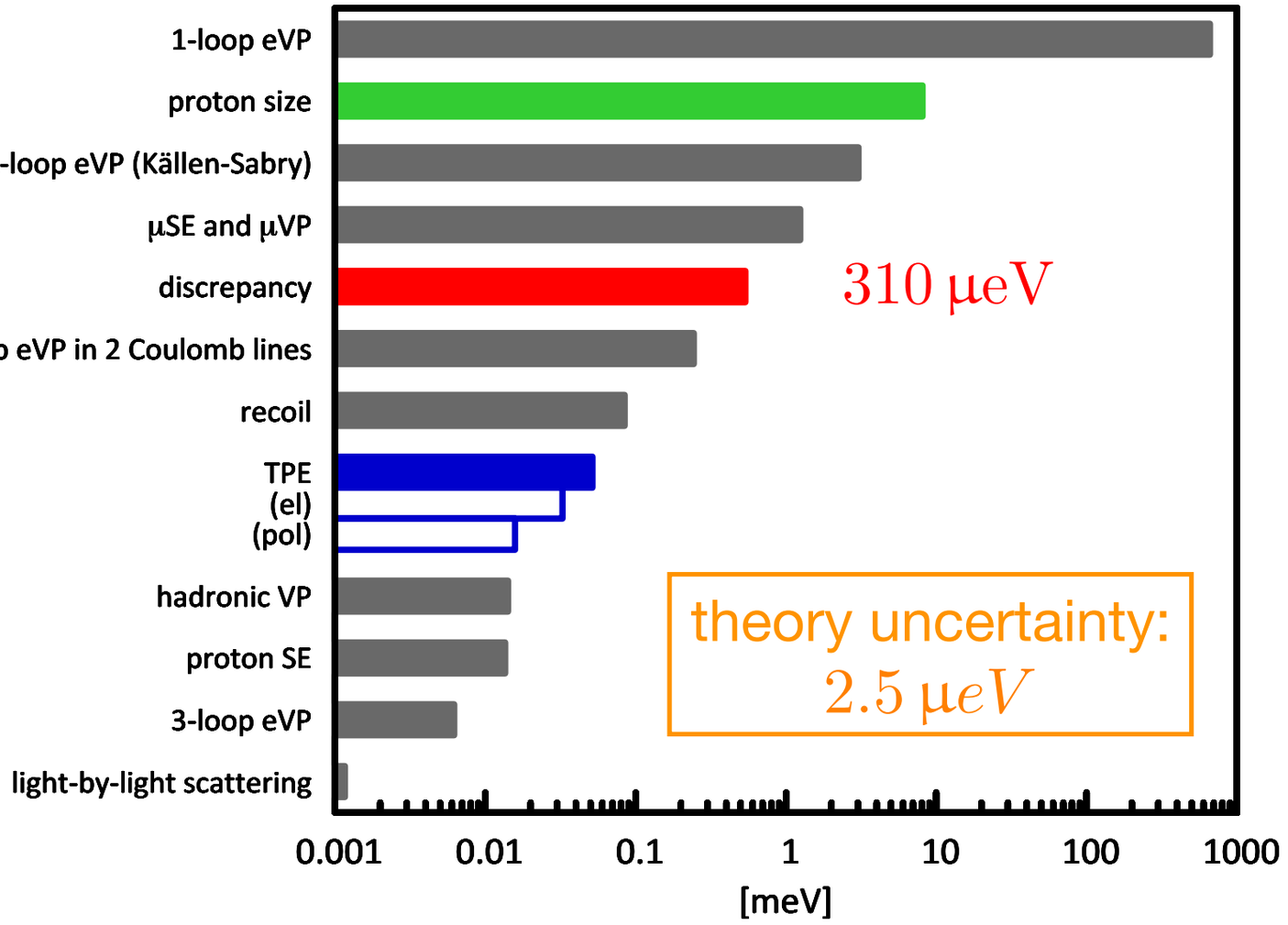

$$E_{\rm LS}^{\mu\rm H\ th.} = 206.0336(15) - 5.2275(10)\left(\frac{R_E}{\rm fm}\right)^2 + E_{\rm LS}^{2\gamma} \qquad \text{[values in meV]}$$

$$E_{\rm LS} = -\frac{\alpha}{12a^3}R_E^2 + \mathcal{O}(\alpha^5)$$

THEORY OF μH LAMB SHIFT

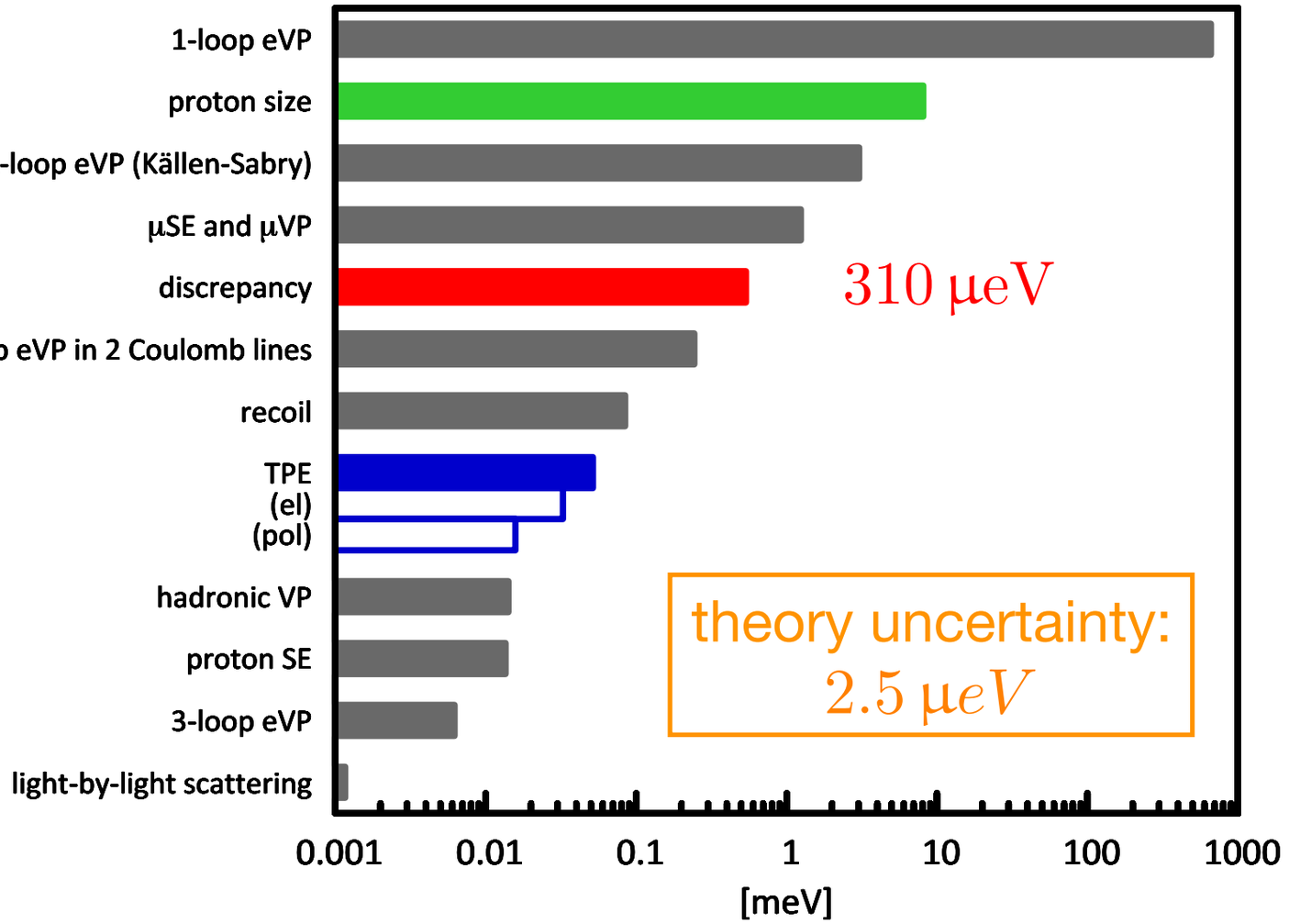

subleading effects of proton structure proposed to resolve the puzzle

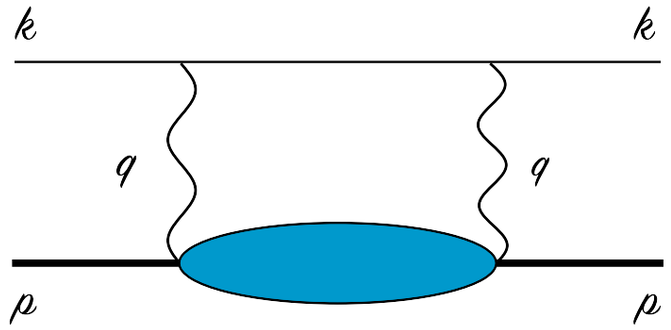

$$\delta V^{(2\gamma)} = \delta V^{(2\gamma)}_{\text{elastic}} + \delta V^{(2\gamma)}_{\text{polariz.}}$$

$$E^{\mu\text{H th.}}_{\text{LS}} = 206.0336(15) - 5.2275(10)\left(\frac{R_E}{\text{fm}}\right)^2 + E^{2\gamma}_{\text{LS}}$$

[values in meV]

$$E_{\text{LS}} = -\frac{\alpha}{12a^3} R_E^2 + \mathcal{O}(\alpha^5)$$

THEORY OF μH LAMB SHIFT

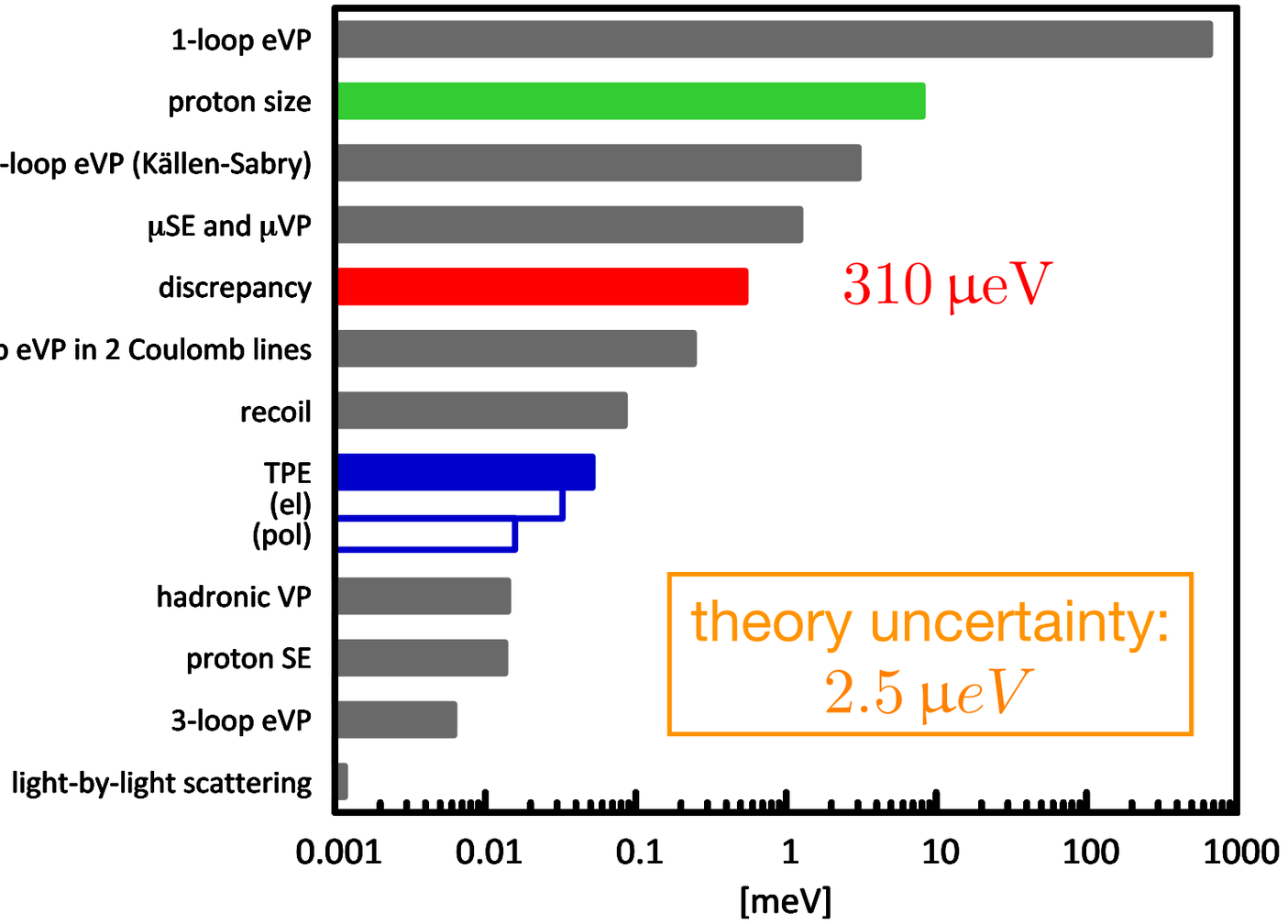

subleading effects of proton structure proposed to resolve the puzzle

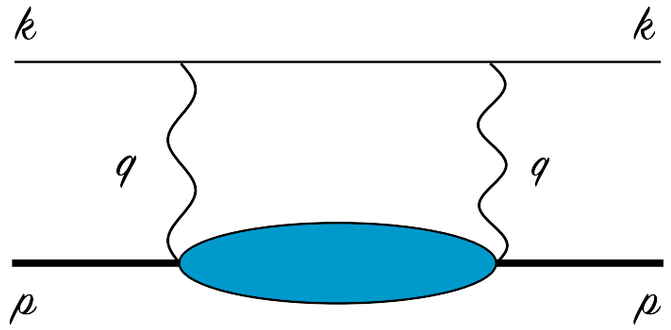

$$\delta V^{(2\gamma)} = \delta V^{(2\gamma)}_{\text{elastic}} + \delta V^{(2\gamma)}_{\text{polariz.}}$$

2γ talk by V. Pascalutsa on Thursday

$$E^{\mu\text{H th.}}_{\text{LS}} = 206.0336(15) - 5.2275(10)\left(\frac{R_E}{\text{fm}}\right)^2 + E^{2\gamma}_{\text{LS}}$$

[values in meV]

$$E_{\text{LS}} = -\frac{\alpha}{12a^3} R_E^2 + \mathcal{O}(\alpha^5)$$

PROTON STRUCTURE IN EP SCATTERING

Photoabsorption cross section:

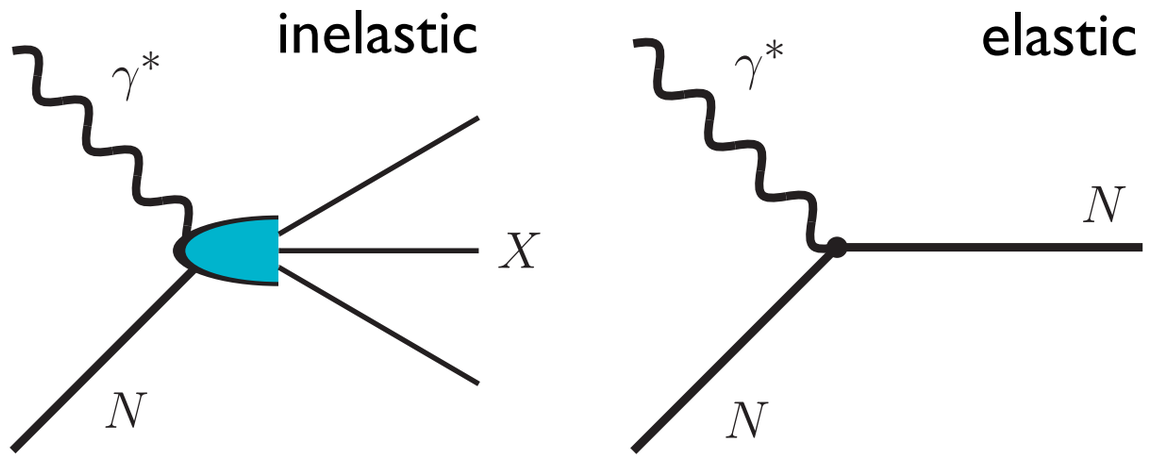

PROTON STRUCTURE IN EP SCATTERING

Photoabsorption cross section:

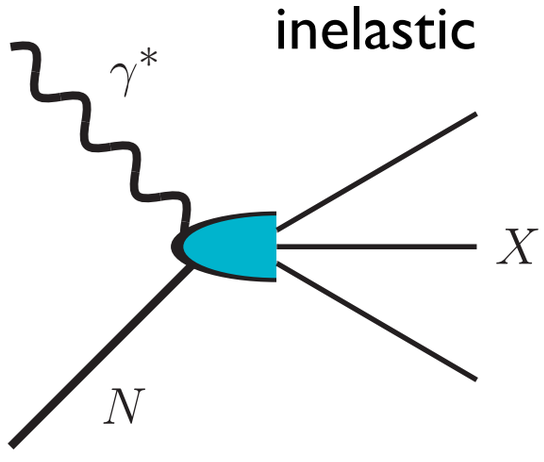

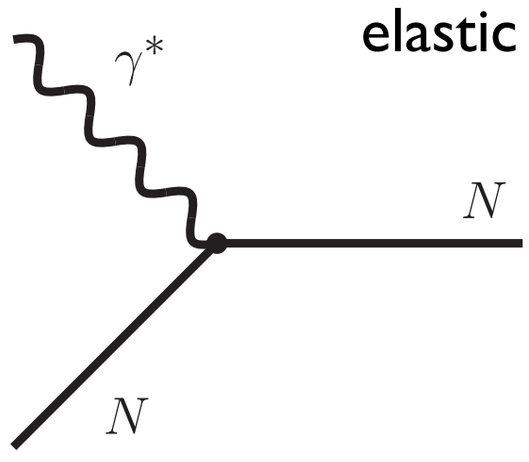

elastic + inelastic
= Born + non-Born

Compton scattering (CS):

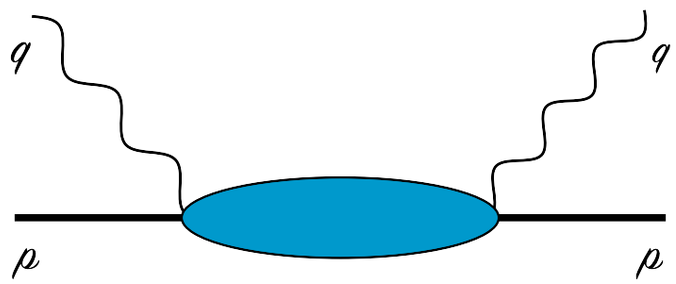

Photon energy and virtuality: ν, Q^2
Bjorken variable: $x = Q^2/2M\nu$
$\tau = Q^2/4M^2$

PROTON STRUCTURE IN EP SCATTERING

Photoabsorption cross section:

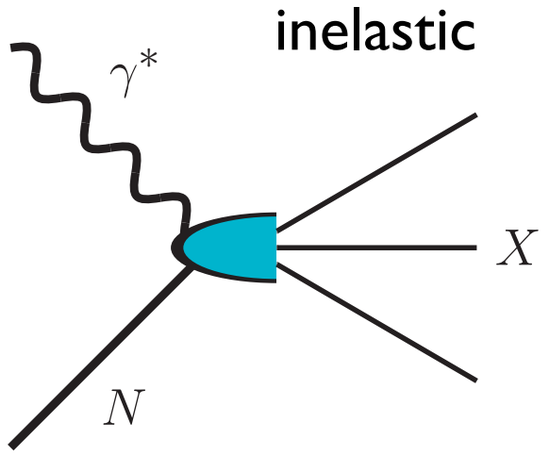

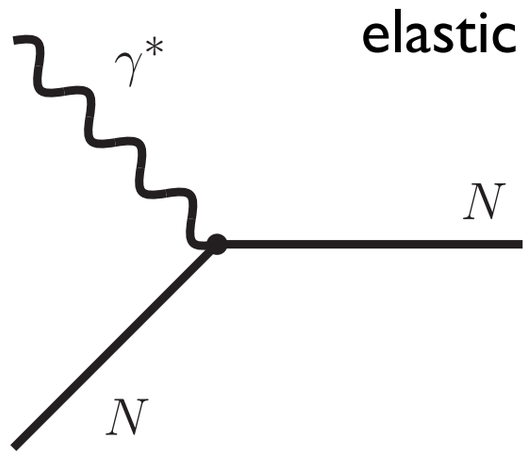

elastic + inelastic
= Born + non-Born

Compton scattering (CS):

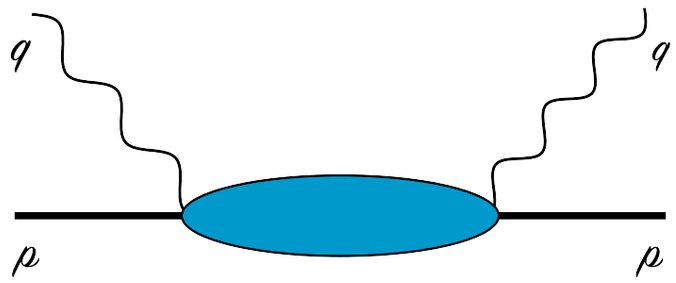

Photon energy and virtuality: ν, Q^2
Bjorken variable: $x = Q^2/2M\nu$
$\tau = Q^2/4M^2$

Proton structure functions:

$$f_1(x,Q^2),\ f_2(x,Q^2),\ g_1(x,Q^2),\ g_2(x,Q^2)$$

Elastic structure functions:

Sachs form factors: G_E, G_M
Dirac & Pauli form factors: F_1, F_2

$$f_1^{\rm el}(x,Q^2) = \frac{1}{2}\,G_M^2(Q^2)\,\delta(1-x)$$
$$f_2^{\rm el}(x,Q^2) = \frac{1}{1+\tau}\left[G_E^2(Q^2) + \tau G_M^2(Q^2)\right]\delta(1-x)$$
$$g_1^{\rm el}(x,Q^2) = \frac{1}{2}\,F_1(Q^2)\,G_M(Q^2)\,\delta(1-x)$$
$$g_2^{\rm el}(x,Q^2) = -\frac{\tau}{2}\,F_2(Q^2)\,G_M(Q^2)\,\delta(1-x)$$

PROTON STRUCTURE IN EP SCATTERING

Photoabsorption cross section:

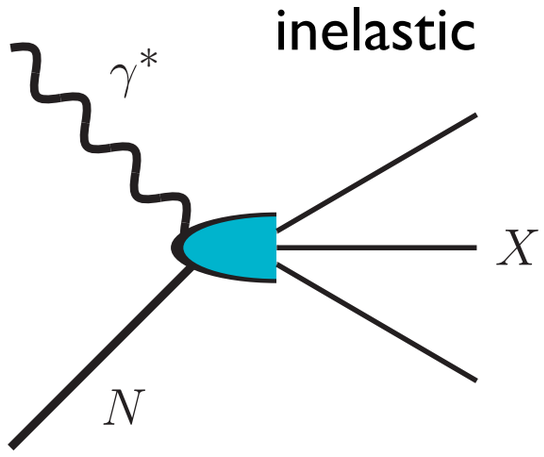

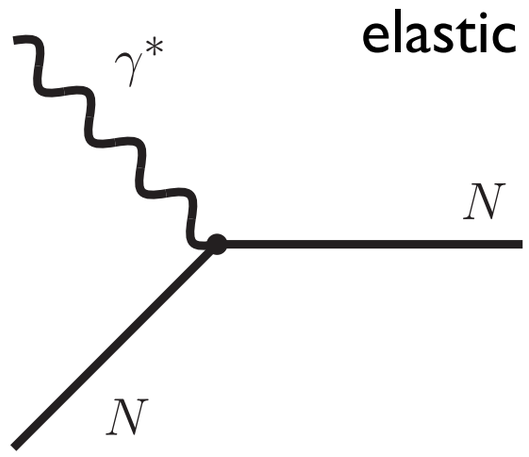

elastic + inelastic
= Born + non-Born

Compton scattering (CS):

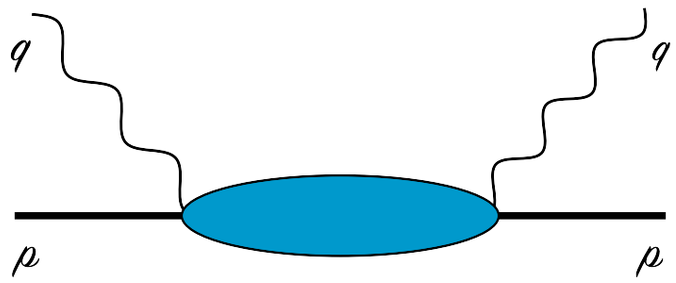

Photon energy and virtuality: ν, Q^2
Bjorken variable: $x = Q^2/2M\nu$
$\tau = Q^2/4M^2$

Proton polarizabilities:

$$\delta_{LT}(Q^2) = \frac{16\alpha M^2}{Q^6} \int_0^{x_0} \mathrm{d}x\, x^2 \big[g_1 + g_2\big](x, Q^2)$$

Proton structure functions:

$$f_1(x, Q^2),\ f_2(x, Q^2),\ g_1(x, Q^2),\ g_2(x, Q^2)$$

Elastic structure functions:

Sachs form factors: G_E, G_M
Dirac & Pauli form factors: F_1, F_2

$$f_1^{\mathrm{el}}(x, Q^2) = \frac{1}{2}\, G_M^2(Q^2)\, \delta(1-x)$$
$$f_2^{\mathrm{el}}(x, Q^2) = \frac{1}{1+\tau} \left[G_E^2(Q^2) + \tau G_M^2(Q^2)\right] \delta(1-x)$$
$$g_1^{\mathrm{el}}(x, Q^2) = \frac{1}{2}\, F_1(Q^2)\, G_M(Q^2)\, \delta(1-x)$$
$$g_2^{\mathrm{el}}(x, Q^2) = -\frac{\tau}{2}\, F_2(Q^2)\, G_M(Q^2)\, \delta(1-x)$$

PROTON STRUCTURE IN EP SCATTERING

Photoabsorption cross section:

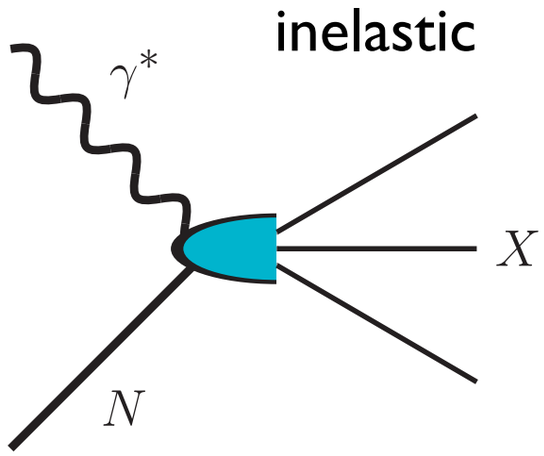

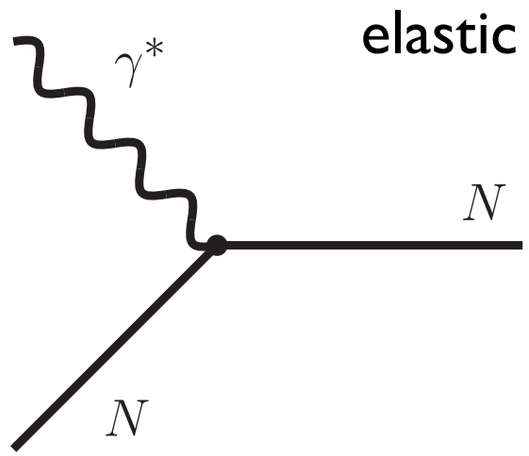

elastic + inelastic
= Born + non-Born

Compton scattering (CS):

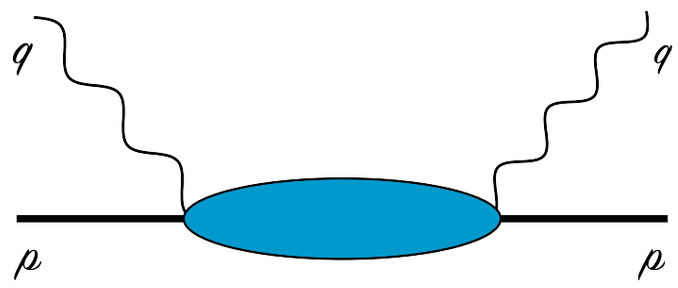

Photon energy and virtuality: ν, Q^2
Bjorken variable: $x = Q^2/2M\nu$
$\tau = Q^2/4M^2$

Proton polarizabilities:

$$\delta_{LT}(Q^2) = \frac{16\alpha M^2}{Q^6}\int_0^{x_0} \mathrm{d}x\, x^2 \big[g_1 + g_2\big](x, Q^2)$$

Proton structure functions:

$f_1(x, Q^2)$, $f_2(x, Q^2)$ — Lamb shift

$g_1(x, Q^2)$, $g_2(x, Q^2)$ — Hyperfine splitting (HFS)

Elastic structure functions:

Sachs form factors: G_E, G_M
Dirac & Pauli form factors: F_1, F_2

$$f_1^{\mathrm{el}}(x, Q^2) = \frac{1}{2}\, G_M^2(Q^2)\, \delta(1-x)$$
$$f_2^{\mathrm{el}}(x, Q^2) = \frac{1}{1+\tau}\left[G_E^2(Q^2) + \tau G_M^2(Q^2)\right] \delta(1-x)$$
$$g_1^{\mathrm{el}}(x, Q^2) = \frac{1}{2}\, F_1(Q^2)\, G_M(Q^2)\, \delta(1-x)$$
$$g_2^{\mathrm{el}}(x, Q^2) = -\frac{\tau}{2}\, F_2(Q^2)\, G_M(Q^2)\, \delta(1-x)$$

STRUCTURE EFFECTS THROUGH 2γ

- Proton-structure effects at subleading orders arise through multi-photon processes

forward
two-photon exchange (2γ)

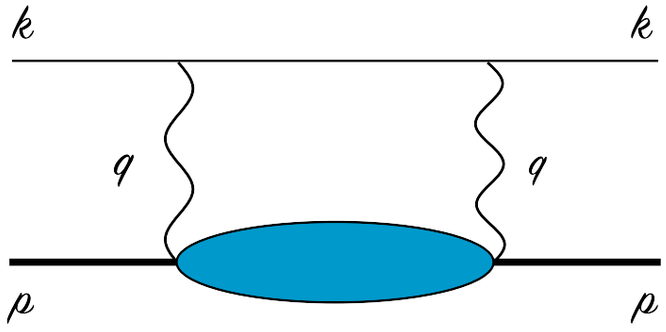

polarizability contribution
(non-Born VVCS)

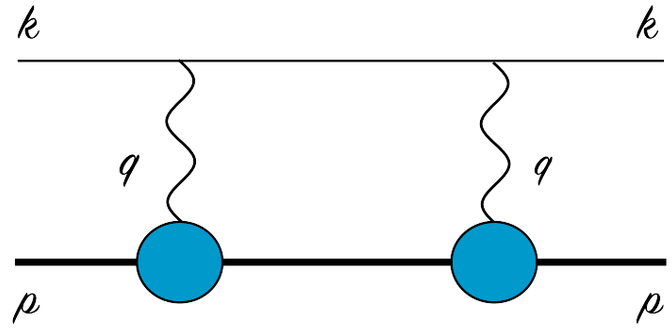

elastic contribution:
finite-size recoil,
3rd Zemach moment (Lamb shift),
Zemach radius (Hyperfine splitting)

STRUCTURE EFFECTS THROUGH 2γ

- Proton-structure effects at subleading orders arise through multi-photon processes

forward
two-photon exchange (2γ)

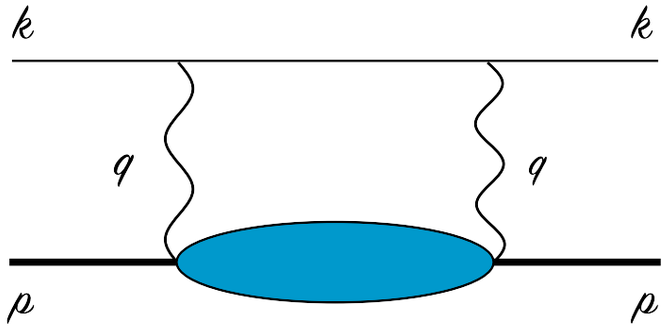

polarizability contribution
(non-Born VVCS)

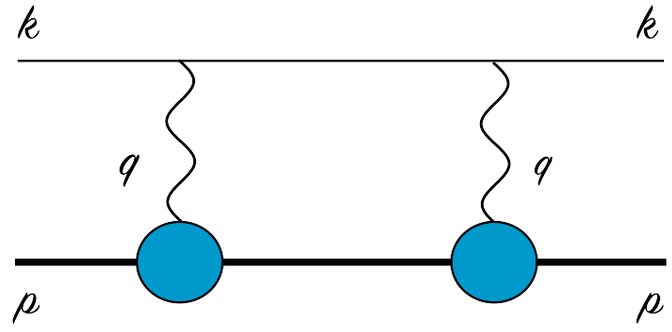

elastic contribution:
finite-size recoil,
3rd Zemach moment (Lamb shift),
Zemach radius (Hyperfine splitting)

- "Blob" corresponds to doubly-virtual Compton scattering (VVCS):

$$T^{\mu\nu}(q,p) = \left(-g^{\mu\nu} + \frac{q^\mu q^\nu}{q^2}\right) T_1(\nu, Q^2) + \frac{1}{M^2}\left(p^\mu - \frac{p\cdot q}{q^2}\, q^\mu\right)\left(p^\nu - \frac{p\cdot q}{q^2}\, q^\nu\right) T_2(\nu, Q^2)$$
$$- \frac{1}{M}\gamma^{\mu\nu\alpha} q_\alpha S_1(\nu, Q^2) - \frac{1}{M^2}\left(\gamma^{\mu\nu} q^2 + q^\mu \gamma^{\nu\alpha} q_\alpha - q^\nu \gamma^{\mu\alpha} q_\alpha\right) S_2(\nu, Q^2)$$

STRUCTURE EFFECTS THROUGH 2γ

- Proton-structure effects at subleading orders arise through multi-photon processes

forward
two-photon exchange (2γ)

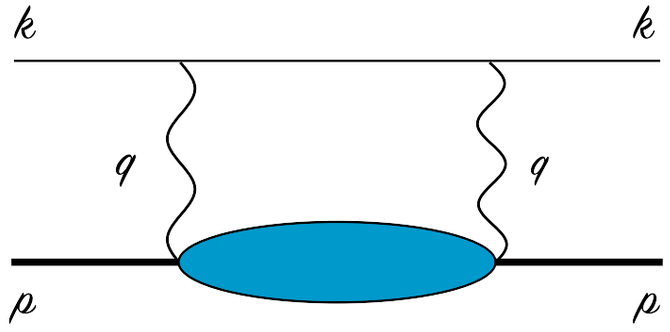

polarizability contribution
(non-Born VVCS)

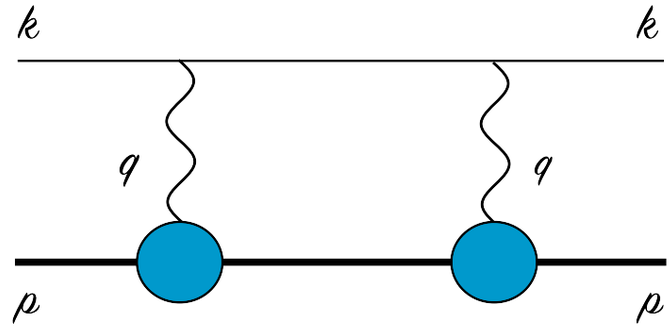

elastic contribution:
finite-size recoil,
3rd Zemach moment (Lamb shift),
Zemach radius (Hyperfine splitting)

- "Blob" corresponds to doubly-virtual Compton scattering (VVCS):

$$T^{\mu\nu}(q,p) = \left(-g^{\mu\nu} + \frac{q^\mu q^\nu}{q^2}\right) \boxed{T_1(\nu, Q^2)} + \frac{1}{M^2}\left(p^\mu - \frac{p\cdot q}{q^2}\, q^\mu\right)\left(p^\nu - \frac{p\cdot q}{q^2}\, q^\nu\right) \boxed{T_2(\nu, Q^2)}$$
$$- \frac{1}{M}\gamma^{\mu\nu\alpha} q_\alpha \boxed{S_1(\nu, Q^2)} - \frac{1}{M^2}\left(\gamma^{\mu\nu} q^2 + q^\mu \gamma^{\nu\alpha} q_\alpha - q^\nu \gamma^{\mu\alpha} q_\alpha\right) \boxed{S_2(\nu, Q^2)}$$

- Proton structure functions: $\boxed{f_1(x,Q^2),\ f_2(x,Q^2)}, \boxed{g_1(x,Q^2),\ g_2(x,Q^2)}$

Lamb shift

Hyperfine splitting (HFS)

2γ EFFECT IN THE LAMB SHIFT

wave function at the origin

$$\Delta E(nS) = 8\pi\alpha m\,\phi_n^2\,\frac{1}{i}\int_{-\infty}^{\infty}\frac{\mathrm{d}\nu}{2\pi}\int\frac{\mathrm{d}\mathbf{q}}{(2\pi)^3}\,\frac{\left(Q^2-2\nu^2\right)T_1(\nu,Q^2)-\left(Q^2+\nu^2\right)T_2(\nu,Q^2)}{Q^4(Q^4-4m^2\nu^2)}$$

dispersion relation & optical theorem:

$$T_1(\nu,Q^2) = T_1(0,Q^2) + \frac{32\pi Z^2\alpha M\nu^2}{Q^4}\int_0^1 \mathrm{d}x\,\frac{x f_1(x,Q^2)}{1-x^2(\nu/\nu_{\mathrm{el}})^2-i0^+}$$

$$T_2(\nu,Q^2) = \frac{16\pi Z^2\alpha M}{Q^2}\int_0^1 \mathrm{d}x\,\frac{f_2(x,Q^2)}{1-x^2(\nu/\nu_{\mathrm{el}})^2-i0^+}$$

2γ EFFECT IN THE LAMB SHIFT

wave function at the origin

$$\Delta E(nS) = 8\pi\alpha m\,\phi_n^2\,\frac{1}{i}\int_{-\infty}^{\infty}\frac{\mathrm{d}\nu}{2\pi}\int\frac{\mathrm{d}\mathbf{q}}{(2\pi)^3}\,\frac{\left(Q^2-2\nu^2\right)T_1(\nu,Q^2)-\left(Q^2+\nu^2\right)T_2(\nu,Q^2)}{Q^4(Q^4-4m^2\nu^2)}$$

dispersion relation & optical theorem:

$$T_1(\nu,Q^2) = \boxed{T_1(0,Q^2)} + \frac{32\pi Z^2\alpha M\nu^2}{Q^4}\int_0^1 \mathrm{d}x\,\frac{x f_1(x,Q^2)}{1-x^2(\nu/\nu_{\mathrm{el}})^2-i0^+}$$

$$T_2(\nu,Q^2) = \frac{16\pi Z^2\alpha M}{Q^2}\int_0^1 \mathrm{d}x\,\frac{f_2(x,Q^2)}{1-x^2(\nu/\nu_{\mathrm{el}})^2-i0^+}$$

- Caution: in the data-driven dispersive approach the $T_1(0,Q^2)$ subtraction function is modelled!

low-energy expansion:

$$\lim_{Q^2\to 0}\overline{T}_1(0,Q^2)/Q^2 = 4\pi\beta_{M1}$$

modelled Q^2 behavior:

$$\overline{T}_1(0,Q^2) = 4\pi\beta_{M1}\,Q^2/\left(1+Q^2/\Lambda^2\right)^4$$

2γ EFFECT IN THE LAMB SHIFT

wave function at the origin

$$\Delta E(nS) = 8\pi\alpha m\,\phi_n^2\,\frac{1}{i}\int_{-\infty}^{\infty}\frac{\mathrm{d}\nu}{2\pi}\int\frac{\mathrm{d}\mathbf{q}}{(2\pi)^3}\,\frac{\left(Q^2-2\nu^2\right)T_1(\nu,Q^2)-\left(Q^2+\nu^2\right)T_2(\nu,Q^2)}{Q^4(Q^4-4m^2\nu^2)}$$

dispersion relation & optical theorem:

$$T_1(\nu,Q^2) = \boxed{T_1(0,Q^2)} + \frac{32\pi Z^2\alpha M\nu^2}{Q^4}\int_0^1 \mathrm{d}x\,\frac{x f_1(x,Q^2)}{1-x^2(\nu/\nu_{\mathrm{el}})^2-i0^+}$$

$$T_2(\nu,Q^2) = \frac{16\pi Z^2\alpha M}{Q^2}\int_0^1 \mathrm{d}x\,\frac{f_2(x,Q^2)}{1-x^2(\nu/\nu_{\mathrm{el}})^2-i0^+}$$

- Caution: in the data-driven dispersive approach the $T_1(0,Q^2)$ subtraction function is modelled!

low-energy expansion:

$$\lim_{Q^2\to 0}\overline{T}_1(0,Q^2)/Q^2 = 4\pi\beta_{M1}$$

modelled Q^2 behavior:

$$\overline{T}_1(0,Q^2) = 4\pi\beta_{M1}\,Q^2/\left(1+Q^2/\Lambda^2\right)^4$$

Assuming ChPT is working, it should be best applicable to atomic systems, where the energies are very small !

2γ POLARIZABILITY EFFECT FROM BCHPT

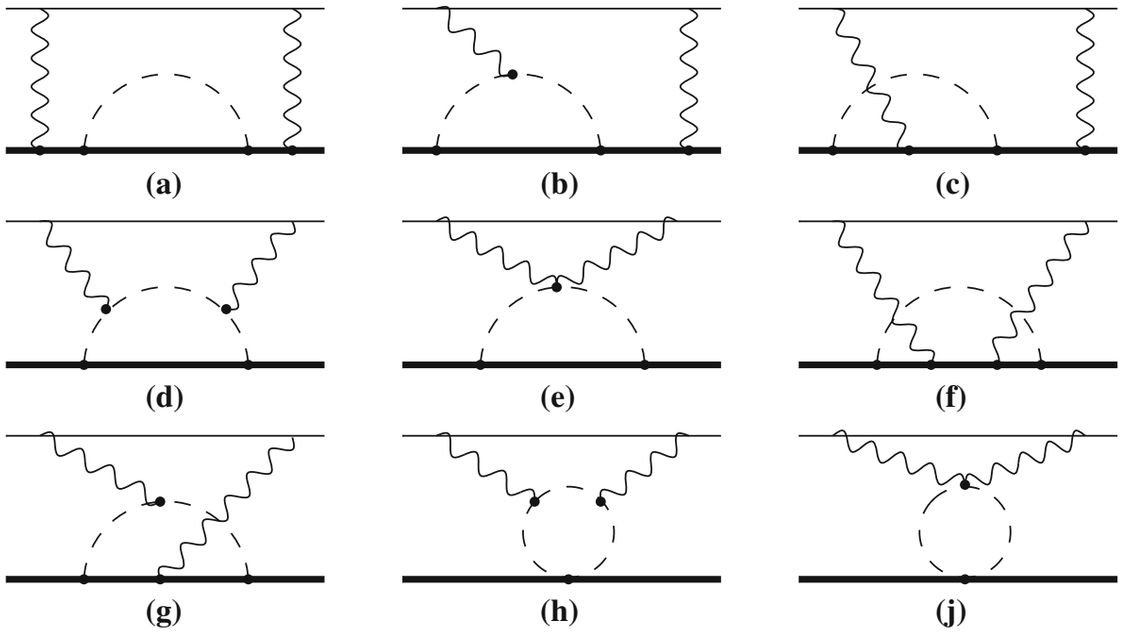

- LO BChPT prediction with pion-nucleon loop diagrams:

$$\Delta E^{\langle \mathrm{LO} \rangle \mathrm{pol}}(2S, \mu\mathrm{H}) = -8.2\,^{+1.2}_{-2.5}\,\mu\mathrm{eV}$$

J. M. Alarcon, V. Lensky, V. Pascalutsa, Eur. Phys. J. C **74** (2014) 2852

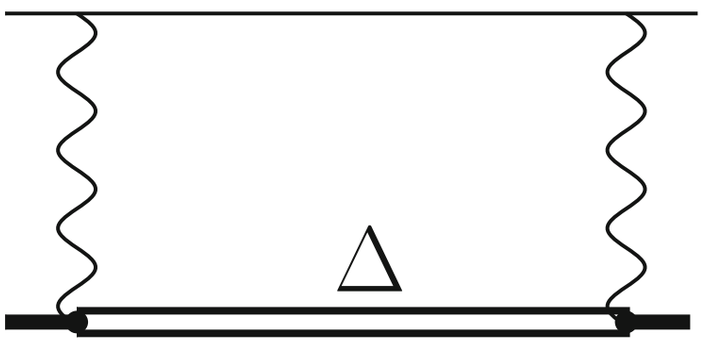

V. Lensky, FH, V. Pascalutsa, M. Vanderhaeghen, Phys. Rev. D **97** (2018) 074012

- Δ prediction from Δ(1232) exchange:
  - Uses large-N_c relations for the Jones-Scadron N-to-Δ transition form factors
  - Small due to the suppression of β_{M1} in the Lamb shift but important for the T_1 subtraction function

$$\Delta E^{\langle \Delta\text{-excit} \rangle \mathrm{pol}}(2S, \mu\mathrm{H}) = 0.95 \pm 0.95\,\mu\mathrm{eV}$$

POLARIZABILITY EFFECT IN LAMB SHIFT

BChPT result is in good agreement with dispersive calculations !!!

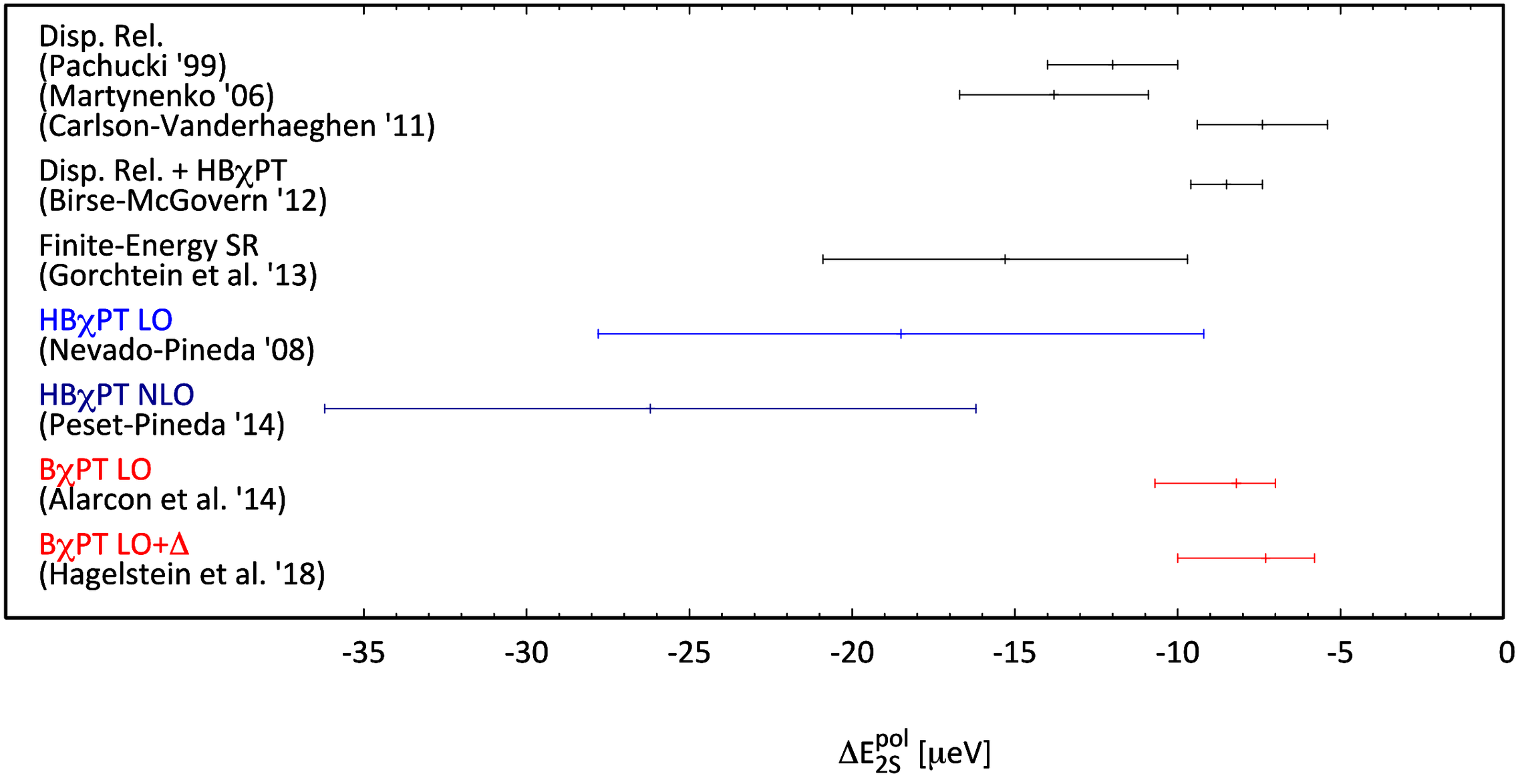

POLARIZABILITY EFFECT IN LAMB SHIFT

BChPT result is in good agreement with dispersive calculations !!!

Agreement also for the contribution of the T_1 subtraction function !!!

TABLE I: Two-photon-exchange contribution to the $2S$-$2P$ Lamb shift in muonic hydrogen. All results are of $\mathcal{O}(\alpha^5)$, i.e., strictly speaking only the S-level shift has been calculated. All energies are in μeV.

Reference	$E_{\rm Born}$	$E_{\rm subt}$	$E_{\rm inel}$	$E_{\rm pol}$	$E^{(5)}_{\rm nucl}(2S)$
Pachucki [40]	$-23.2(1.0)$	1.9	-13.9	$-12(2)$	$-35.2(2.2)$
Martynenko [42]		2.3	-16.1	$-13.8(2.9)$	
Carlson & Vanderhaeghen [25]	$-29.5(1.3)$	5.3(1.9)	$-12.7(5)$	$-7.4(2.0)$	$-36.9(2.4)$
Birse & McGovern [27]	$-24.7(1.6)^a$	4.2(1.0)	$-12.7(5)^b$	$-8.5(1.1)$	$-33(2)$
Gorchtein et al. [29]^c	$-24.5(1.2)$	$-2.3(4.6)$	$-13.0(6)$	$-15.3(4.6)$	$-39.8(4.8)$
Hill et al. [26, 33]	-18.4	1.1(13.0)	$-12.7(5)^b$	$-11.6(13.0)$	$-30.0(13.0)$
Tomalak [31, 41]^d	$-18.6(1.6)$	2.3(1.3)	$-12.7(5)^b$	$-10.3(1.4)$	$-29.0(2.1)$
Pineda et al. [23, 24, 30, 43]	$-8.3(4.3)$	$2.85(1.20)^e$		$-26.2(10.0)$	$-34.4(12.5)$
Hagelstein et al. [28, 44]		$4.6^{+2.3}_{-2.4}$	$-11.8^{+2.1}_{-2.5}$	$-7.3^{+1.5}_{-2.7}$	

[a] Result taken from Ref. [25] with reinstated "non-pole" Born piece.

[b] Value taken from Ref. [25].

[c] Adjusted values; the original values of Ref. [29], $E_{\rm subt} = 3.3$ and $E_{\rm Born} = -30.1$, are based on a different decomposition into elastic and polarizability contributions.

[d] The charge radius r_C is taken from μH spectroscopy.

[e] This number is obtained if the contribution from Fig. 3 is subtracted, otherwise this term diverges. See the discussion in Sec. IV.

HYPERFINE SPLITTING IN μH

$$\Delta E_{\mathrm{HFS}}(nS) = [1 + \Delta_{\mathrm{QED}} + \Delta_{\mathrm{weak}} + \Delta_{\mathrm{structure}}]\, E_F(nS)$$

with $\Delta_{\mathrm{structure}} = \Delta_Z + \Delta_{\mathrm{recoil}} + \Delta_{\mathrm{pol}}$

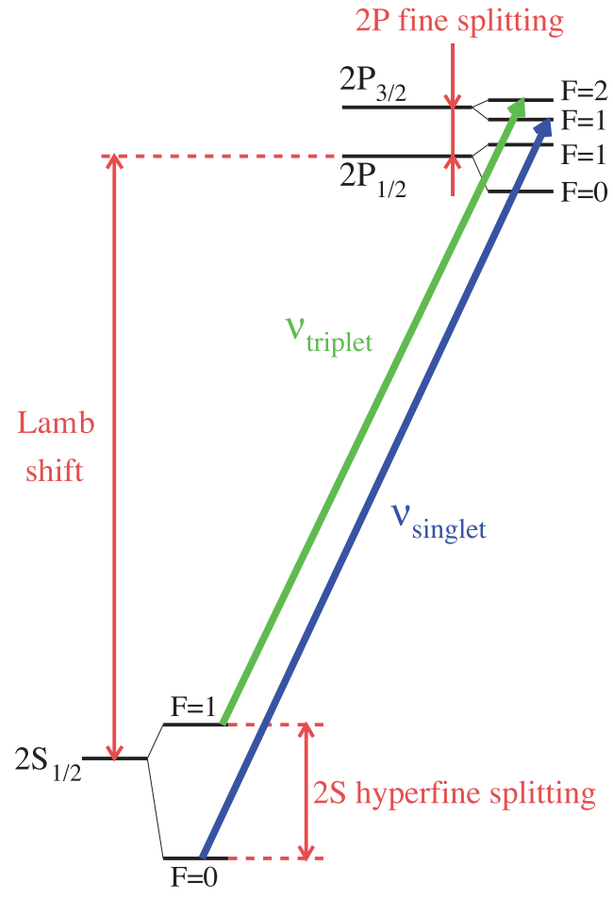

HYPERFINE SPLITTING IN μH

$$\Delta E_{\rm HFS}(nS) = [1 + \Delta_{\rm QED} + \Delta_{\rm weak} + \Delta_{\rm structure}]\, E_F(nS)$$

with $\Delta_{\rm structure} = \boxed{\Delta_Z} + \Delta_{\rm recoil} + \Delta_{\rm pol}$

Zemach radius:

$$\Delta_Z = \frac{8Z\alpha m_r}{\pi} \int_0^\infty \frac{{\rm d}Q}{Q^2} \left[\frac{G_E(Q^2) G_M(Q^2)}{1+\kappa} - 1 \right] \equiv -2Z\alpha m_r R_Z$$

experimental value: $R_Z = 1.082(37)\,{\rm fm}$

A. Antognini, et al., Science **339** (2013) 417–420

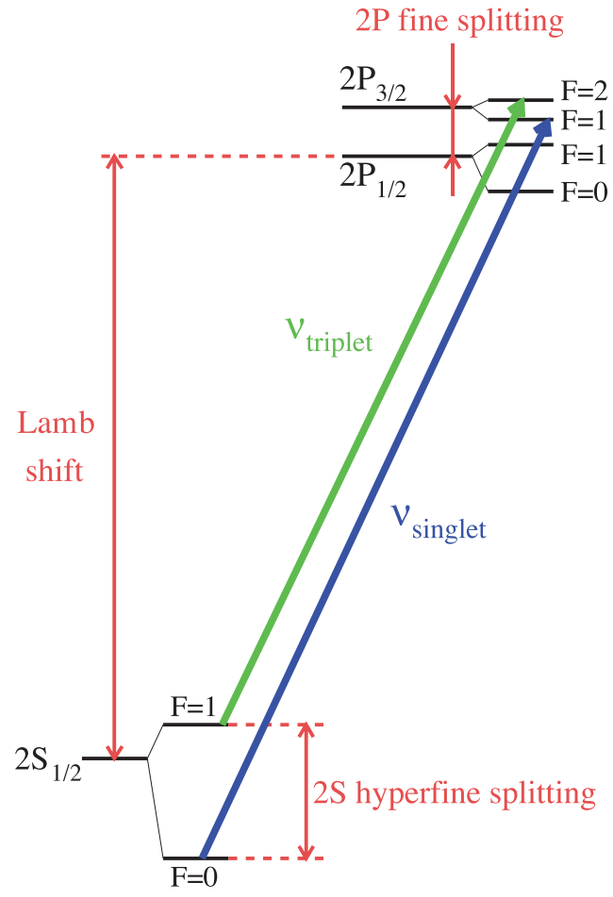

HYPERFINE SPLITTING IN μH

$$\Delta E_{\mathrm{HFS}}(nS) = [1 + \Delta_{\mathrm{QED}} + \Delta_{\mathrm{weak}} + \Delta_{\mathrm{structure}}]\, E_F(nS)$$

with $\Delta_{\mathrm{structure}} = \Delta_Z + \Delta_{\mathrm{recoil}} + \Delta_{\mathrm{pol}}$

Zemach radius:

$$\Delta_Z = \frac{8Z\alpha m_r}{\pi} \int_0^\infty \frac{\mathrm{d}Q}{Q^2} \left[\frac{G_E(Q^2) G_M(Q^2)}{1+\kappa} - 1 \right] \equiv -2Z\alpha m_r R_Z$$

experimental value: $R_Z = 1.082(37)\,\mathrm{fm}$

A. Antognini, et al., Science **339** (2013) 417–420

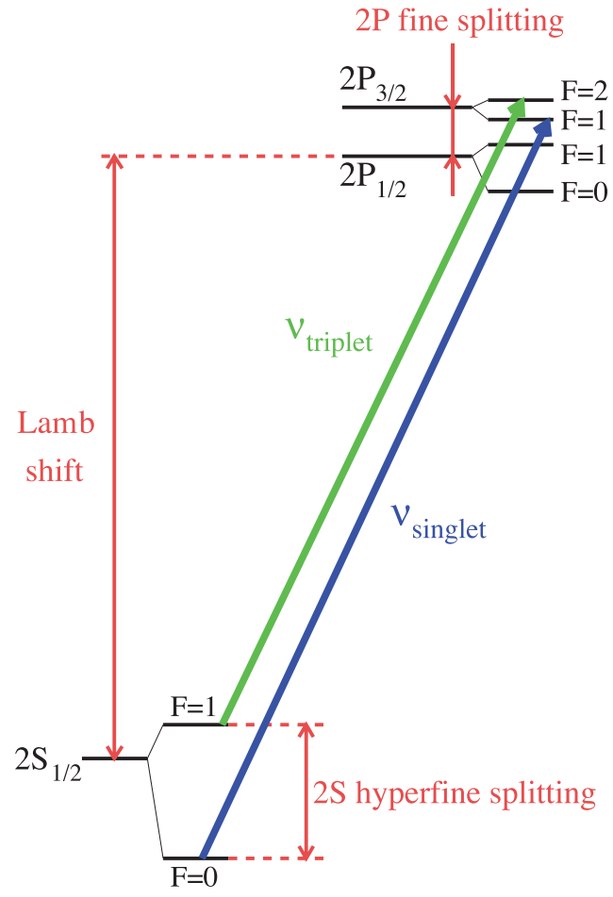

⏰ Measurements of the μH ground-state HFS planned by the CREMA, FAMU and J-PARC / Riken-RAL collaborations

HYPERFINE SPLITTING IN μH

$$\Delta E_{\rm HFS}(nS) = [1 + \Delta_{\rm QED} + \Delta_{\rm weak} + \Delta_{\rm structure}]\, E_F(nS)$$

with $\Delta_{\rm structure} = \Delta_Z + \Delta_{\rm recoil} + \Delta_{\rm pol}$

Zemach radius:

$$\Delta_Z = \frac{8Z\alpha m_r}{\pi} \int_0^\infty \frac{{\rm d}Q}{Q^2} \left[\frac{G_E(Q^2) G_M(Q^2)}{1+\kappa} - 1 \right] \equiv -2Z\alpha m_r R_Z$$

experimental value: $R_Z = 1.082(37)\,{\rm fm}$

A. Antognini, et al., Science **339** (2013) 417–420

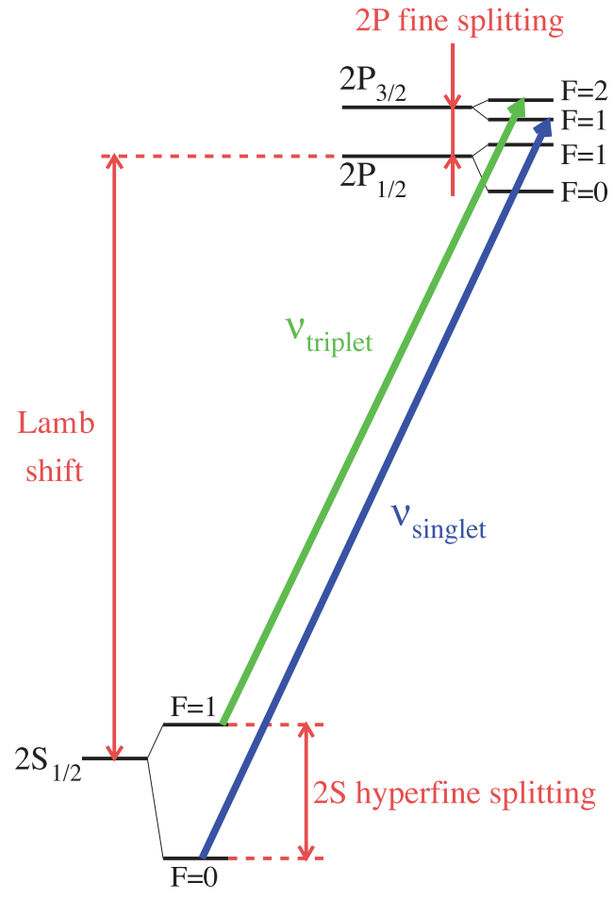

- Measurements of the μH ground-state HFS planned by the CREMA, FAMU and J-PARC / Riken-RAL collaborations
- Very precise input for the 2γ polarizability effect needed to find the μH ground-state HFS transition in experiment

HYPERFINE SPLITTING IN μH

$$\Delta E_{\mathrm{HFS}}(nS) = [1 + \Delta_{\mathrm{QED}} + \Delta_{\mathrm{weak}} + \Delta_{\mathrm{structure}}]\, E_F(nS)$$

with $\Delta_{\mathrm{structure}} = \Delta_Z + \Delta_{\mathrm{recoil}} + \Delta_{\mathrm{pol}}$

Zemach radius:

$$\Delta_Z = \frac{8Z\alpha m_r}{\pi} \int_0^\infty \frac{\mathrm{d}Q}{Q^2} \left[\frac{G_E(Q^2) G_M(Q^2)}{1+\kappa} - 1 \right] \equiv -2Z\alpha m_r R_Z$$

experimental value: $R_Z = 1.082(37)\ \mathrm{fm}$

A. Antognini, et al., Science **339** (2013) 417–420

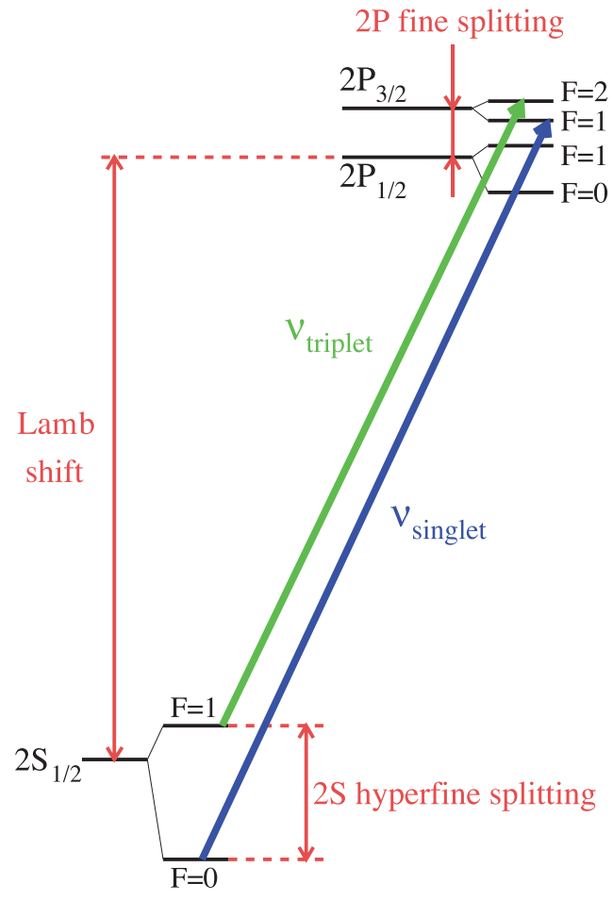

- Measurements of the μH ground-state HFS planned by the CREMA, FAMU and J-PARC / Riken-RAL collaborations
- Very precise input for the 2γ polarizability effect needed to find the μH ground-state HFS transition in experiment
- Zemach radius can help to pin down the magnetic properties of the proton

2γ POLARIZABILITY EFFECT IN THE HFS

$$\Delta_{\rm pol} = \frac{\alpha m}{2\pi(1+\kappa)M}\left[\Delta_1 + \Delta_2\right]$$

$$\Delta_1 = 2\int_0^\infty \frac{{\rm d}Q}{Q}\left(\frac{5+4v_l}{(v_l+1)^2}\left[4I_1(Q^2)+F_2^2(Q^2)\right] - \frac{32M^4}{Q^4}\int_0^{x_0}{\rm d}x\, x^2 g_1(x,Q^2)\right.$$
$$\left.\times\left\{\frac{1}{(v_l+\sqrt{1+x^2\tau^{-1}})(1+\sqrt{1+x^2\tau^{-1}})(1+v_l)}\left[4+\frac{1}{1+\sqrt{1+x^2\tau^{-1}}}+\frac{1}{v_l+1}\right]\right\}\right)$$

$$\Delta_2 = 96M^2\int_0^\infty\frac{{\rm d}Q}{Q^3}\int_0^{x_0}{\rm d}x\, g_2(x,Q^2)\left\{\frac{1}{v_l+\sqrt{1+x^2\tau^{-1}}}-\frac{1}{v_l+1}\right\}$$

- Polarizability effect on the HFS is completely constrained by empirical information
- ChPT calculation will put the reliability of dispersive calculations (and ChPT) to the test ?!

2γ POLARIZABILITY EFFECT IN THE HFS

$$\Delta_{\rm pol} = \frac{\alpha m}{2\pi(1+\kappa)M}\,[\Delta_1 + \Delta_2]$$

$$\Delta_1 = 2\int_0^\infty \frac{{\rm d}Q}{Q}\left(\frac{5+4v_l}{(v_l+1)^2}\left[4I_1(Q^2)+F_2^2(Q^2)\right] - \frac{32M^4}{Q^4}\int_0^{x_0}{\rm d}x\,x^2 g_1(x,Q^2)\right.$$
$$\left.\times\left\{\frac{1}{(v_l+\sqrt{1+x^2\tau^{-1}})(1+\sqrt{1+x^2\tau^{-1}})(1+v_l)}\left[4+\frac{1}{1+\sqrt{1+x^2\tau^{-1}}}+\frac{1}{v_l+1}\right]\right\}\right)$$

$$\Delta_2 = 96M^2\int_0^\infty\frac{{\rm d}Q}{Q^3}\int_0^{x_0}{\rm d}x\,g_2(x,Q^2)\left\{\frac{1}{v_l+\sqrt{1+x^2\tau^{-1}}}-\frac{1}{v_l+1}\right\}$$

- Polarizability effect on the HFS is completely constrained by empirical information
- ChPT calculation will put the reliability of dispersive calculations (and ChPT) to the test ?!

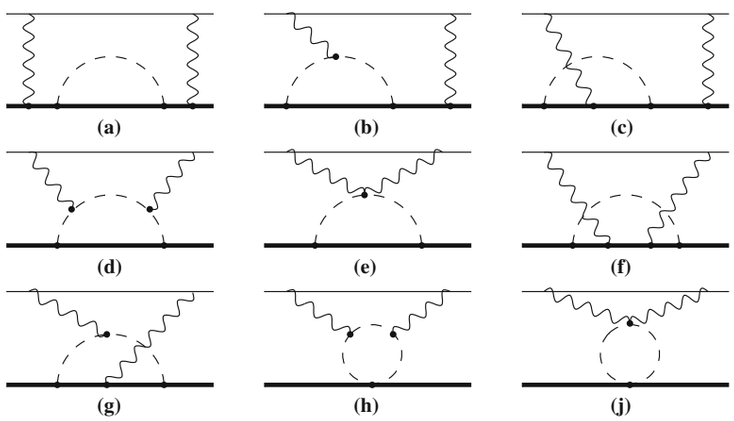

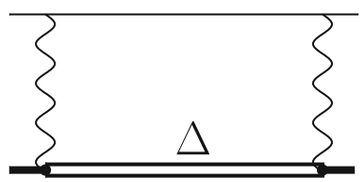

$$E_{\rm HFS}^{\langle {\rm LO}\rangle {\rm pol}}(2S,\mu{\rm H}) = 0.9(2.2)\,\mu{\rm eV}$$
$$E_{\rm HFS}^{\langle \Delta-{\rm excit}\rangle {\rm pol}}(2S,\mu{\rm H}) = -\,1.2(8)\,\mu{\rm eV}$$

POLARIZABILITY EFFECT IN HFS

Tension between the BChPT prediction and data-driven dispersive results !!!

- Δ_2 predictions based on MAID and most recent Hall B models are very different as compared to the Hall B 2007 model (talk by K. Slifer at ECT*, 02.07.18)

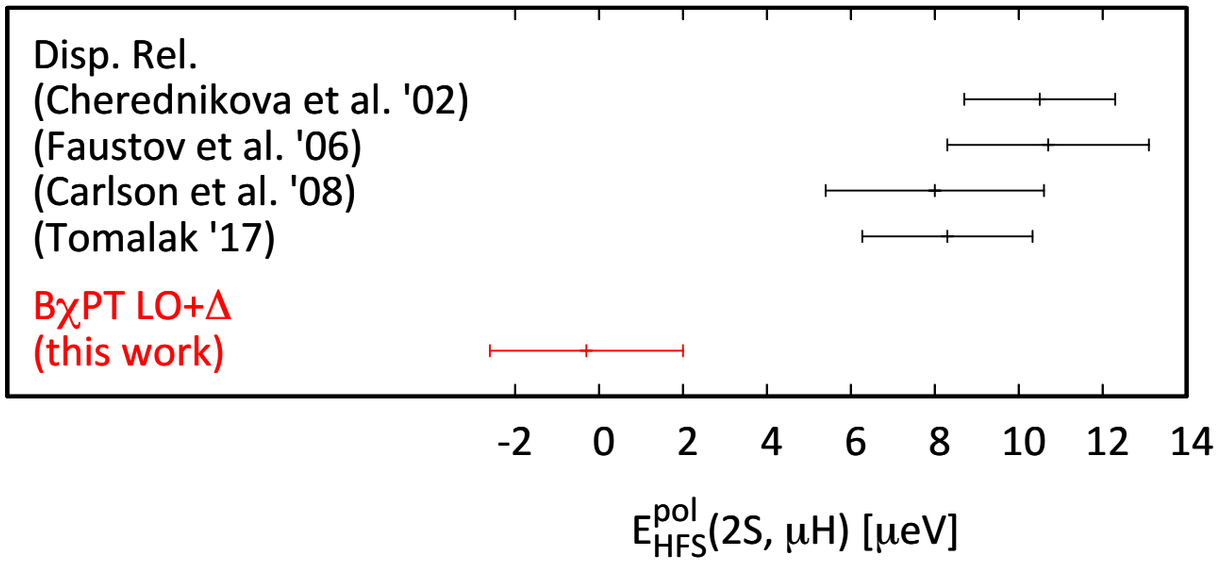

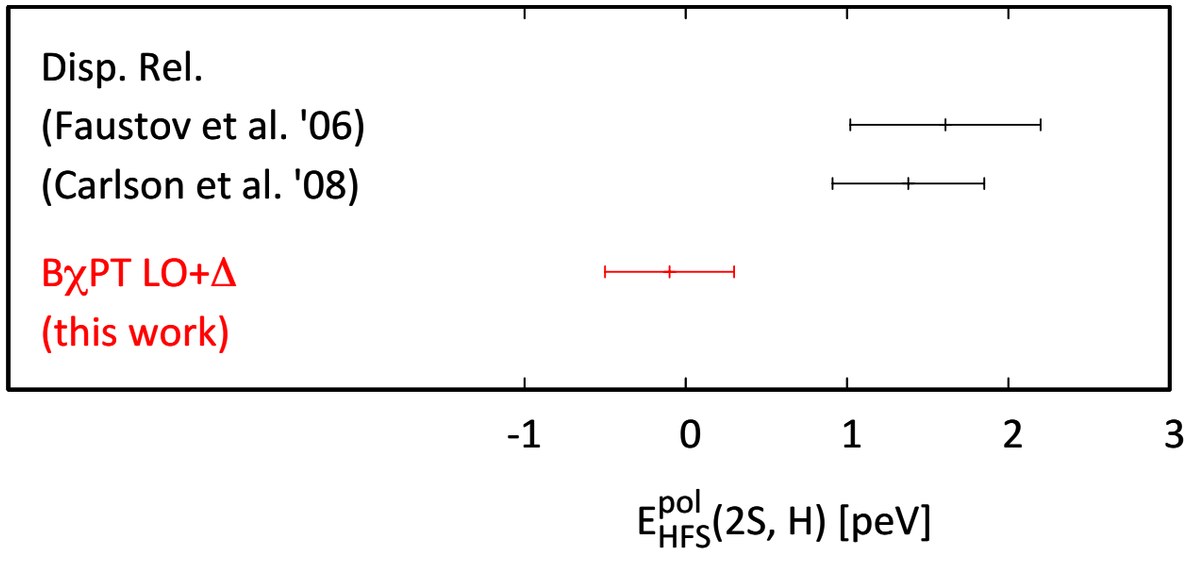

- Changes the Zemach radius extraction (smaller, just like R_E)
- Empirical information on spin structure functions is limited (especially for g_2)
- Low-Q region is very important (cancelation between I_1 and F_2)

SUMMARY HYPERFINE SPLITTING

TABLE III: Two-photon-exchange contribution to the $2S$ hyperfine splitting in muonic hydrogen, see Eq. (31). All energies are given in meV. The hyperfine splitting for a proton with structure is E_{HFS}; the hyperfine splitting without two-photon exchange is $\left[E_{HFS} - E_{HFS}^{(5)}\right]$.

Reference	$E_F(2S)\,\Delta_Z$	$E_F(2S)\,\Delta_R$	$E_F(2S)\,\Delta_{pol}$	$E_{HFS}^{(5)}(2S)$	$E_{HFS}(2S)$	$\left[E_{HFS} - E_{HFS}^{(5)}\right](2S)$
Pachucki [2]	−0.183	0.038	0.000(15)	−0.145	22.745(15)	22.890
Martynenko et al. [74, 80][a]	−0.1518		0.0093	−0.1425	22.8136(78)	22.9561
Faustov et al. [81][a]			0.0095(24)			
Carlson et al. [35, 36][b]	−0.1731	0.0190	0.0080(26)	−0.1460(32)	22.8146(49)	22.9606
Tomalak [73][c]	−0.1672(11)	0.0193(1)	0.0083(20)	−0.1396(24)	22.8146(26)	22.9542
Tomalak [41, 71]				−0.1410(11)	22.8132(15)	22.9542
Peset & Pineda [64]					22.8123(33)	
Hagelstein et al. [79]			−0.0003(23)			
Experiment [7]					22.8089(51)	

[a] Adjusted value; as suggested in Ref. [36], the original polarizability contribution is corrected by adding $-1.2\,\mu$eV because the conventions of "elastic" and "inelastic" contributions applied in Ref. [74] are inconsistent.

[b] With proton form factors from Ref. [75]. The corrections Δ_Z and Δ_R of Refs. [35, 36] are converted to definitions of this Section.

[c] The charge radius r_C is taken from μH spectroscopy.

SUMMARY AND CONCLUSION

Lower-bound function: $R_E^2(Q^2) = -\frac{6}{Q^2}\log G_E(Q^2)$

- Finite Q^2 data can be used to establish a rigorous lower bound on the proton charge radius, while bypassing the model-dependent assumptions that go into the fitting and extrapolation of the electron-proton scattering data

SUMMARY AND CONCLUSION

Lower-bound function: $R_E^2(Q^2) = -\frac{6}{Q^2}\log G_E(Q^2)$

- Finite Q^2 data can be used to establish a rigorous lower bound on the proton charge radius, while bypassing the model-dependent assumptions that go into the fitting and extrapolation of the electron-proton scattering data

- Determinations of the 2γ proton-polarizability contributions based on BCHPT or the data-driven dispersive approach agree for the Lamb Shift but disagree for the hyperfine splitting

- Very precise input for the 2γ polarizability effect needed to find the μH ground-state hyperfine splitting in experiment